Mon. Not. R. Astron. Soc. **000**, 1–18 (2010) Printed 15 April 2010 (MN LATEX style file v2.2)

# Mass transport by buoyant bubbles in galaxy clusters

Edward C.D. Pope[1⋆], Arif Babul[1], Georgi Pavlovski[2], Richard G. Bower[3], Aaron Dotter[1]
[1] *Department of Physics & Astronomy, University of Victoria, Victoria, BC, V8P 1A1, Canada*
[2] *School of Physics & Astronomy, University of Southampton, Southampton, SO17 1BJ, UK*
[3] *Institute for Computational Cosmology, Department of Physics, Durham University, South Road, Durham DH1 3LE, UK*



15 April 2010

**ABSTRACT**

We investigate the effect of three important processes by which AGN-blown bubbles transport material: drift, wake transport and entrainment. The first of these, drift, occurs because a buoyant bubble pushes aside the adjacent material, giving rise to a net upward displacement of the fluid behind the bubble. For a spherical bubble, the mass of upwardly displaced material is roughly equal to half the mass displaced by the bubble, and should be $\sim 10^{7-9}\,\mathrm{M}_{\odot}$ depending on the local ICM and bubble parameters. We show that in classical cool core clusters, the upward displacement by drift may be a key process in explaining the presence of filaments behind bubbles. A bubble also carries a parcel of material in a region at its rear, known as the wake. The mass of the wake is comparable to the drift mass and increases the average density of the bubble, trapping it closer to the cluster centre and reducing the amount of heating it can do during its ascent. Moreover, material dropping out of the wake will also contribute to the trailing filaments. Mass transport by the bubble wake can effectively prevent the build-up of cool material in the central galaxy, even if AGN heating does not balance ICM cooling. Finally, we consider entrainment, the process by which ambient material is incorporated into the bubble. Studies of observed bubbles show that they subtend an opening angle much larger than predicted by simple adiabatic expansion. We show that bubbles that entrain ambient material as they rise, *will* expand faster than the adiabatic prediction; however, the entrainment rate required to explain the observed opening angle is large enough that the density contrast between the bubble and its surroundings would disappear rapidly. We therefore conclude that entrainment is unlikely to be a dominant mass transport process. Additionally, this also suggests that the bubble surface is much more stable against instabilities that promote entrainment than expect for pure hydrodynamic bubbles.

**Key words:**

## 1 INTRODUCTION

The hot, gaseous atmospheres of galaxy clusters often show depressions in the X-ray surface brightness (see, for example McNamara 2002; Bîrzan et al. 2004; Dunn et al. 2005; Rafferty et al. 2006). These depressions are indicative of empty cavities, or bubbles, embedded in the hot gas (e.g. McNamara & Nulsen 2007). The presence of bubbles is generally taken to be a signature of AGN feedback. In this model, a fraction of the material cooling from the gaseous atmosphere is accreted by a supermassive black hole located in the central galaxy. This releases vast amounts of energy often in the form of outflows which couple to the hot atmosphere (e.g. Churazov et al. 2002; Benson & Babul 2009).

AGN feedback is widely considered to have important consequences for the evolution of single galaxies, as well as galaxy groups and clusters. For example, feedback is thought to be key in determining the upper mass cut-off of the galaxy mass function (Benson et al. 2003; Croton et al. 2006; Bower et al. 2006), balancing the radiative losses in cool-core galaxy clusters, as well as providing the non-gravitational 'pre-heating' that may be important for non cool-core clusters (e.g. Babul et al. 2002; McCarthy et al. 2004, 2008). Feedback also seems to play a role in determining the relationship between the temperature and X-ray luminosity of hot atmospheres across a range of halo masses (Babul et al. 2002; McCarthy et al. 2004; Puchwein et al. 2008; Bower et al. 2008; Davé et al. 2008; Pope 2009). As a direct consequence, feedback also regulates supermassive black hole growth (e.g. Silk & Rees 1998; Churazov et al.

⋆ E-mail:ecdpope@uvic.ca

2005) and, therefore, its relation to the properties of the host galaxy.

Considerable effort has been invested in understanding the impact of supermassive black holes. One of the key challenges is understanding how the energy from the AGN affects and couples to the broader environment. Most studies that have sought to describe this relationship have focused on bulk motion, shock waves and pressure/gravity waves induced by AGN outbursts and the subsequent dissipation of the associated energy (see McNamara & Nulsen 2007, for a review). In this article we focus on the transport of material out of the cluster centre by AGN-blown bubbles. As an example, the filaments of cool material observed behind AGN-blown bubbles (e.g. Conselice et al. 2001; Crawford et al. 2005; Hatch et al. 2006) are a strong indication of bubble-induced mass transport within several 10s of kiloparsecs of the cluster centre. The most obvious example is the Perseus cluster in which the filaments contain some $10^8$ solar masses of cool material (e.g. Salomé et al. 2006, 2008). More generally, some of the transport mechanisms we discuss in this paper may carry matter out to $\sim$100 kiloparsecs from the cluster centre.

Mass transport by bubbles not only reduces the amount of material available for forming new stars in the central galaxy, allowing the normally adopted stringent requirement that AGN heating perfectly balance cooling to be some relaxed, but also affects the bubble dynamics and energetics. Hence, a better understanding of the main mass transport mechanisms is essential for describing the energy balance in the ICM. Here, we focus on three important processes by which bubbles can transport material: drift, wake transport and the entrainment of ambient material into the bubble.

The aim of this article is to quantitatively describe these three main mechanisms and also the corresponding implications. The discussion is largely analytical, intended to facilitate a better understanding of the underappreciated aspects of these mechanisms and aid in the interpretation of both observations and numerical simulations.

The article is arranged in the following way. Section 2 outlines the basic bubble model that serves as a backdrop for subsequent discussions. Sections 3, 4 and 5 focus on each of the three mechanisms — drift, wake transport and entrainment. In each section, we discuss a process as well as associated, potentially observable consequences, like trailing optical filaments. In Section 6, we consider how mass transport modifies the ongoing debate about whether or not AGN heating need balance cooling precisely. We summarize our key findings in Section 7.

## 2 BUBBLE MODEL

The magnitude and spatial extent of mass transport associated with buoyant bubbles depend heavily on the dynamics and the energetics of the bubble. It is, therefore, essential to have a model which accurately describes these processes.

In broad brushstrokes, an AGN-inflated bubble is believe to evolve as follows: an AGN jet inflates a bubble of what is generally assumed to be relativistic fluid in the intracluster medium. The details of the inflation process itself are not well understood and models for the bubble inflation range from nearly adiabatic to supersonic. In either case, at the end of the inflation process, the bubble is expected to be in pressure equilibrium with its surroundings. As a result of the mass density in the bubble being lower than that of the ambient medium, the bubble is buoyant and will rise, moving away from the AGN and in the case of galaxy clusters, the cluster centre, towards more distant regions of lower density and pressure. The velocity of the bubble is determined by the near balance between buoyancy and drag forces with the ICM. In response to dropping ambient pressure, the bubble will expand. The end stage of bubble evolution is not well understood. One possibility is that the bubble will be destroyed during the rise by hydrodynamical (Raleigh-Taylor and Kelvin-Helmholtz) instabilities; however, it is equally plausible that ambient conditions (magnetic fields on the bubble surface or viscosity in the ICM) suppress these instabilities, allowing the bubble to rise to a radius where the bubble density becomes equal to that of its environment, and buoyancy force vanishes. In the latter case, the bubble of relativistic fluid will hover at its equilibrium height as a "ghost cavity", invisible in the X-rays though it may still be detectable in low frequency radio observations.

In the context of mass transport, the most important stage in the evolution of the bubble is the second (or the rise) phase. The dynamics and thermodynamics of this particular phase have been discussed widely (e.g. Churazov et al. 2002; Enßlin & Heinz 2002; Mathews et al. 2003; Nusser et al. 2006; Nulsen et al. 2007). Typically, most analyses assume that the rise velocity of the bubble is sufficiently slow such that the response of the medium internal to the bubble to the bubble expansion is adiabatic. This approximation yields reasonable theoretical expectations.

In addition, most treatments also assume that the bubble density is much less than that of the surrounding ICM and derive the relevant relationships in the limit of an extreme density contrast. For many of the calculations, this approximation is probably adequate. However, the density contrast determines the maximum height to which the bubble rises, and so is critical for determining the magnitude and the spatial scale of the mass transport phenomenon, as well as the efficiency with which energy can be extracted from the bubble. As we will discuss in the following sections, mass transport processes endow a bubble with an effective — and in the case of entrainment, a real — finite density contrast. A more complete description of bubble dynamics and thermodynamics must therefore allow for a finite density contrast. At relevant sections of this paper, we will therefore present modified relationships governing bubble dynamics and thermodynamics that takes into account this aspect.

## 3 BUBBLE DRIFT AND TRAILING COOL FILAMENTS

As a bubble rises, energy conservation requires that the change in its gravitational potential energy is accompanied by a gain in kinetic energy of the bubble and the ICM. The latter is induced by the ICM being pushed by the rising bubble, causing a net upward displacement behind the bubble. This phenomenon is known as "drift" (Darwin 1953) [1] Fig-

[1] The phenomenon of drift is utilised in industrial mixing processes, called fluidised beds, which are formed when gas is passed

ure 1 depicts a schematic view of the bubble and its trailing drift (e.g. Crowe 2005; Yang 2003; Schetz & Fuhs 1999).

Drift is closely related to the better-known concept of "added mass" (e.g. Nusser et al. 2006; Pavlovski et al. 2007), a concept associated with moving bodies submerged in a fluid. The usual interpretation is that it represents the increased inertia associated with the work required to change the kinetic energy of the fluid flow around the body. The ambient fluid can be thought of as increasing the effective mass of the moving object (e.g. Milne-Thompson 1996).

In group and cluster environments, this trailing fluid can, under certain conditions, give rise to filaments of cool gas. In this section, we introduce the phenomenon of drift, discuss the associated characteristics, and explore whether the recently discovered optical filaments stretching between the AGN-inflated bubbles and the cluster centres (e.g. Conselice et al. 2001; Crawford et al. 2005; Salomé et al. 2006; Hatch et al. 2006) are related to the drift. The kinematic data (e.g. Hatch et al. 2006) certainly suggests that the filaments may well be the result of cool material that was originally lifted from the cluster center and that some of this material is now falling back.

### 3.1 Drift: a conceptual outline

Darwin (1953) considered the problem of a body moving uniformly through an infinite, inviscid, incompressible fluid. Importantly, Darwin studied the motion in the fluid frame of reference rather than the rest frame of the body in which the fluid particles follow simple streamlines. In the fluid frame, the trajectories are extremely complex, consisting of a large-scale looping motion and a permanent displacement in the direction of body's motion.

The forward displacement occurs because a moving body pushes the fluid ahead of it causing the fluid to move in the same direction as the body. In due course, the forward-displaced fluid slows down, though in the situation considered by Darwin (1953) never formally comes to rest behind the body. As an illustration, one can imagine a rising bubble approaching and traversing a stationary marked plane within the fluid column, oriented at right angles to its direction of motion. As the bubble passes through the plane, the fluid will be displaced upwards in the horn-like shape depicted in the third panel figure 1, with the fluid closer to the body experiencing a greater net translation.

Strictly speaking, the fluid displacement has two contributions: $X_{\rm d}$, a localised (positive) drift contribution which decays rapidly from the body, and $X_{\rm r}$, a non-local (negative) reflux contribution which depends on the far-field boundary conditions and which decays slowly from the body. In the limit that the body starts infinitely far from the marked plane and then moves through the plane to infinity, the reflux contribution is zero, so that the drift volume is single-valued.

In the absence of gravity, the fluid displacement is permanent and the length of the drift grows continuously while the total volume remains approximately constant. However, for drift behind buoyant bubbles in the intracluster environment, the stratification of the fluid cannot be neglected. Not only will gravity bring the drifting fluid particles to rest sooner, it can also potentially cause the fluid to fall back to its original position. As a result, in a stratified fluid, the upward displacement of material due to drift is always finite. The implications of drift in a stratified fluid are described in detail in the next subsection. Presently, we will assume, for simplicity's sake, that the effects of gravity can be neglected.

The volume of fluid enclosed by the intial plane of marked fluid and the distorted plane is called the drift volume, $V_{\rm drift}$, and is depicted in figure 1. In an unbounded flow, it is calculated from the integral of the permanent displacement of fluid particles in the direction of the body's motion over the cross-sectional area of the flow (e.g. Eames & Gilbertson 2005).

The displacement is given by the time integral of the relative velocity between the fluid in the drift and the fluid at infinity. It is calculated from the velocity potential for a uniform flow of an incompressible, non-rotational fluid past a sphere, e.g. Landau & Lifschitz (1995) (see also Pavlovski et al. 2007; Dursi & Pfrommer 2008, for recent examples). Using this, Darwin (1953) showed that the drift and body volumes are related by a constant of proportionality, $k$, which depends on the geometry of the body; for a solid sphere, $k = 0.5$. In the case where bubbles deform completely into vortex rings, Dabiri (2006) found $k = 0.72$, so the value of $k$ for an ordinary bubble should be somewhere between these limiting cases. For generality, we will use (e.g. Milne-Thompson 1996; Schetz & Fuhs 1999)

$$V_{\rm drift} = k(V_{\rm bub} + V_{\rm wake}), \tag{1}$$

where $V_{\rm wake}$ is the wake volume. (For a full list of parameters and constants, see the Appendix A.) Darwin (1953) was also able to show, quite generally, that the mass within the drift volume is equal to the added mass, so that

$$M_{\rm drift} = k\rho_{\rm ICM}(V_{\rm bub} + V_{\rm wake}) \approx kM_{\rm dis}, \tag{2}$$

where $M_{\rm dis}$ is the ICM mass displaced by the bubble.

At the onset of the rise phase, the (initial) displaced mass can be estimated as $M_{\rm dis,0} = \rho_0 V_0$. Given the enthalpy of the bubble at the end of inflation and the beginning of the rise phase

$$E_{\rm bub,0} = \frac{P_0 V_{\rm bub,0}}{\Gamma_{\rm b} - 1} + P_0 V_{\rm bub,0} = \frac{\Gamma_{\rm b}}{\Gamma_{\rm b} - 1} P_0 V_{\rm bub,0}, \tag{3}$$

where $\Gamma_{\rm b}$ is the adiabatic index of the bubble material, we can write

$$M_{\rm dis,0} = \frac{(\Gamma_{\rm b} - 1)}{\Gamma_{\rm b}} \frac{\mu m_{\rm p}}{k_{\rm B} T_0} E_{\rm bub,0} \approx 10^8 \left(\frac{E_{\rm bub,0}}{10^{59}\,{\rm erg}}\right)\left(\frac{T_0}{10^7\,{\rm K}}\right)^{-1} {\rm M}_\odot. \tag{4}$$

Here, $T_0$ is the ambient temperature where the bubble is inflated and we have assumed that the bubble contents are relativistic, hence $\Gamma_{\rm b} = 4/3$. We note that the actual value of $\Gamma_{\rm b}$ will depend on the initial composition of the AGN outflow and whether the jet and the bubble inflation process entrains a significant amount of material from the ICM into the bubble. We will comment on this further when we consider entrainment.

To estimate the drift mass that we would expect to be associated with an AGN-inflated bubble, we assume that

into a vessel containing a bed of solid particles. At a given gas injection rate, a stream of bubbles appears and rises through the bed with tails of material behind them and thereby intensifying mixing (e.g. Crowe 2005; Yang 2003).

**Table 1.** Typical values of phenomenological constants

| Parameter | Plausible Range | Best guess |
|---|---|---|
| k | 0-1 | $\sim 0.5$ |
| q | 0-1 | $\sim 0.24$ |
| $C_{\rm D}$ | $> 0.45$ | $> 0.45$ |
| $\alpha$ | 0-1 | $\lesssim 0.05$ |

$k = 0.5$ since the bubbles tend to generally be more or less spherical. Accordingly, we would expect observations to show a total mass of a few $\times 10^7$ to $\sim 10^8\,{\rm M}_\odot$ of material trailing behind typical bubbles. This value agrees reasonably well with estimates of the mass in the recently discovered cool filaments that stretch between the bubbles and the cluster centre (e.g Salomé et al. 2008).

In principle, it is possible to estimate $k$ for an AGN-blown bubble directly from numerical simulations. Illustrative examples of the characteristic drift signature in galaxy cluster simulations can be found in Revaz et al. (2008); Roediger et al. (2007), though we note that this effect can also be induced by circular vortex lines, which stretch bubbles into tori (e.g. Pavlovski et al. 2007). Furthermore, Churazov et al. (2001) also estimated the mass of material uplifted by their simulated hydrodynamic bubble to be $\sim 10^8\,{\rm M}_\odot$. This agreement is encouraging; however, we do caution that until we achieve a better understanding of the ICM microphysics (including a realistic treatment of magnetic fields, thermal conduction and viscosity) any estimate for $k$ based on numerical simulations is unlikely to significantly improve upon the values quoted above. The same reasoning applies to three other phenomenological parameters used throughout this article: (1) $q$, the fraction of displaced mass trapped in the bubble wake; (2) $C_{\rm D}$, the bubble drag coefficient; (3) $\alpha$, the entrainment coefficient. Plausible ranges and best estimates are given in table 1.

Finally, we note that drift is enhanced at low Reynolds numbers, as can be seen in the viscous hydrodynamic simulations presented by Reynolds et al. (2004). However the theory is much more complex as the drift volume does not have a well-defined maximum as well as being dependent on boundaries in the system (see Eames et al. 2003).

### 3.2 Observed cool optical filaments: a by-product of the drift?

Optical filaments behind bubbles tend to be linear trails of cool material that extend for tens of kiloparsecs towards the cluster centre (e.g. Conselice et al. 2001; Crawford et al. 2005; Salomé et al. 2006; Hatch et al. 2006). These structures are a strong indication of bubble-induced mass transport within several 10s of kiloparsecs of the cluster centre. The mass associated with the filaments is estimated, in Perseus cluster at least, to be $\sim 10^8$ solar masses of cool material (e.g. Salomé et al. 2006, 2008).

The simplest explanation for the filaments is that AGN-blown bubbles lift cool material from the cluster centre when they detach and start to rise. The filaments would appear to grow when some of this material decouples from the bubble-drift system and falls back inward. Filamentary material close to the bubble would, in this picture, still be travelling upward with respect to the cluster centre, while material further away would be travelling towards the cluster centre. The filament would then appear to be stretching, as indicated by observations (e.g. Hatch et al. 2006).

The observable properties of filaments correspond quite closely to the general characteristics of drift. We, therefore, investigate the circumstances under which these processes may produce flows that might be identifiable as filaments. Further to this, we also investigate additional processes which may explain the clumpiness of filaments on scales of tenths of kiloparsecs.

As previously mentioned, the stratification of the ICM exerts a non-negligible influence on motions generated within it. The numerous different flow regimes can be described by using the characteristic length scales of the system. Pertaining to drift behind buoyant bubbles, two useful scales are the Ozmidov and buoyancy lengths. The first parameter relates to the maximum size of turbulent eddies in a stratified fluid. Motions on larger spatial scales, therefore, cannot be turbulent alone and material will also be transported vertically in the fluid. Consequently, the Ozmidov length marks a characteristic scale of fluid motion above which a filament may form behind a buoyant bubble.

The scale length of vertical fluid motion is given by the buoyancy length, which represents the complete conversion of vertical kinetic energy to potential energy in a stratified fluid. It can be seen that filaments will be formed if the buoyancy length exceeds the Ozmidov length. These scales are considered in more detail below.

To a reasonable approximation, the Ozmidov scale can be calculated in the following manner: the kinetic energy per unit mass required to displace a stably stratified fluid a vertical distance $\Delta z$ is of order $\Delta z^2 N^2$, where $N$ is the Brunt-Väisälä (buoyancy) frequency, while the energy associated with turbulence on the same spatial scale is $(\epsilon \Delta z)^{2/3}$, with $\epsilon$ being the energy dissipation rate per unit mass. Equating the kinetic energies gives the Ozmidov scale (e.g. Kantha & Clayson 2000)

$$L_{\rm O} = \left( \frac{\epsilon}{N^3} \right)^{\frac{1}{2}}. \tag{5}$$

where

$$N^2 = -\frac{g}{z} \frac{{\rm d} \ln \sigma}{{\rm d} \ln z}, \tag{6}$$

with $g$ being the gravitational acceleration and $\sigma = P \rho_{\rm ICM}^{-\Gamma_{\rm e}}$ being the entropy index of the ICM. It follows that, in a stratified fluid, there is a maximum kinetic energy associated with the eddies that occur as a consequence of a given body's motion. Therefore, for objects that generate vertical disturbances on scales larger than $L_{\rm O}$, the turbulent eddies cannot dissipate the kinetic energy. Instead, the majority of the kinetic energy goes towards increasing the potential energy of the ICM by carrying denser material from closer to the cluster centre out to larger distances. Motion on much greater scales than $L_{\rm O}$, is expected to generate gravity waves (c.f. Omma et al. 2004). In contrast, for fluid disturbances that are smaller than $L_{\rm O}$, turbulent eddies are highly efficient at disrupting the column of material displaced by drift, thereby preventing an appreciable change in the potential energy of the fluid - in this case no filament will form.

The Ozmidov scale, therefore, marks the transition from

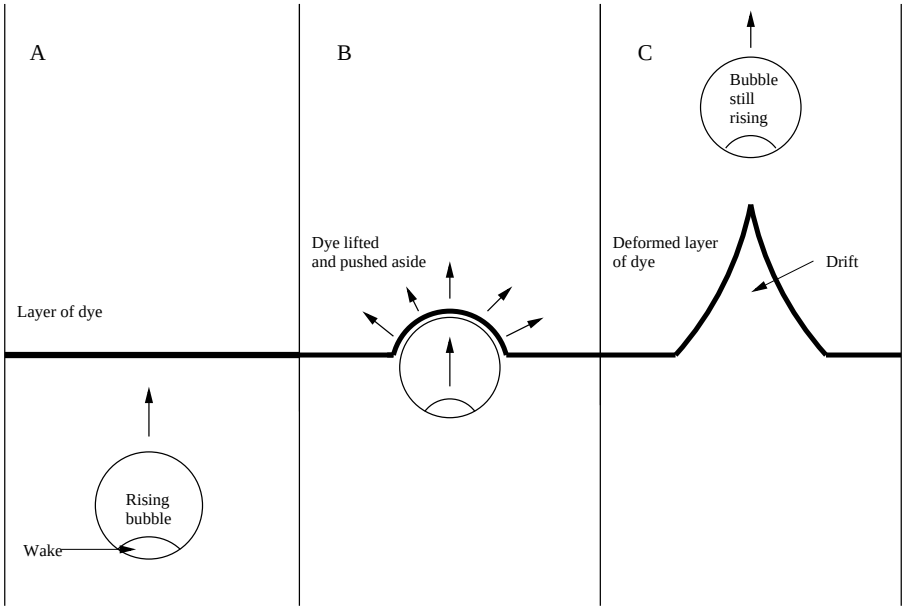


**Figure 1.** Schematic showing wake transport and drift due to passage of bubble. In panel (A) the bubble approaches an initially planar dye surface from below. (B) Distortion of the dye surface occurs as the bubble passes through the plane. (C) The volume between initial plane and horn-like distorted surface is the drift volume.

motions that primarily generate turbulence to those that transport mass vertically. Since turbulence is associated with heating, the transition is equivalent to defining a threshold above which buoyant bubbles predominantly transport mass and below which they generate turbulence, which leads to heating. At this point it is also important to note that if the Ozmidov scale becomes comparable to the size of the smallest eddies, the Kolmogorov scale (e.g. Choudhuri 1998), then turbulence cannot exist in the fluid. This is because the eddy kinetic energy is insufficient to circulate in the direction of the fluid stratification. However, unless the ICM viscosity exceeds the Spitzer value this is unlikely to be the case in clusters of galaxies.

To simplify the expression for $L_{\rm O}$, the turbulent dissipation rate for the bubble is taken to be $\epsilon = c_{\rm turb} w^3/r$ (e.g. Dennis & Chandran 2005), where $c_{\rm turb}$ is a numerical constant, $w$ is the bubble velocity, and $r$ is the bubble radius. In order to describe the scaling properties of the Ozmidov length we will assume that the bubble ascends at its terminal velocity governed by the balance between buoyancy and drag, with a magnitude given by (e.g. Churazov et al. 2001)

$$w_{\rm terminal} = \left(\frac{8rg}{3C_{\rm D}}\right)^{\frac{1}{2}}, \tag{7}$$

where $C_{\rm D}$ is the drag coefficient. For brevity, equation (7) is written $w_{\rm terminal} = (c_{\rm term} rg)^{1/2}$ and the Ozmidov scale can be expressed as

$$L_{\rm O} \approx c_{\rm turb}^{\frac{1}{2}} c_{\rm term}^{\frac{3}{4}} r^{\frac{1}{4}} z^{\frac{3}{4}} \left(\frac{{\rm d}\ln\sigma}{{\rm d}\ln z}\right)^{-\frac{3}{4}}, \tag{8}$$

where $z$ is the bubble's displacement from the cluster centre.

Equation (8) must be compared to the buoyancy length to determine whether filaments actually form. The buoyancy length is defined as the displacement of a fluid parcel at which all its vertical kinetic energy is converted to potential energy. As before, the kinetic energy per unit mass, $w^2$, will displace fluid in a stably stratified atmosphere by a vertical distance $L_{\rm buoy}$, is of order $L_{\rm buoy}^2 N^2$, so that (e.g. Kantha & Clayson 2000) the buoyancy length is

$$L_{\rm buoy} = \frac{w}{N}. \tag{9}$$

For a bubble travelling at its terminal velocity $w = (c_{\rm term} rg)^{1/2}$ (e.g. Churazov et al. 2001), and

$$L_{\rm buoy} \approx c_{\rm term}^{\frac{1}{2}} r^{\frac{1}{2}} z^{\frac{1}{2}} \left(\frac{{\rm d}\ln\sigma}{{\rm d}\ln z}\right)^{-\frac{1}{2}}. \tag{10}$$

Following the discussion in Dennis & Chandran (2005), our constant $c_{\rm turb} = 0.42/2 = 0.21$. Then, using the fact that, for a spherical bubble $c_{\rm term} = 8/(3C_{\rm D})$, it can be shown that filaments can form behind buoyant bubbles provided

$$\frac{L_{\rm buoy}}{L_{\rm O}} \approx 1.7 C_{\rm D}^{\frac{1}{4}} \left(\frac{r}{z}\right)^{\frac{1}{4}} \left(\frac{{\rm d}\ln\sigma}{{\rm d}\ln z}\right)^{\frac{1}{4}} > 1. \tag{11}$$

Whether the criterion above is satisfied depends on the values given to the phenomenological constants, $c_{\rm term}$ and $C_{\rm D}$, as well as observable parameters. It is particularly difficult to assign a characteristic value for the drag coefficient, $C_{\rm D}$, since it depends on both the Mach and Reynolds numbers of the flow (e.g. see Pope et al. 2008, and references therein), which are dependent on the nature of the ICM. Estimating such parameters by comparison with numerical hydrodynamic simulations is not necessarily representative. However, a suitable guess can be obtained in the limit that $C_{\rm D}$ behaves as a conventional drag coefficient so that it varies from $C_{\rm D} \approx 30$ for a Reynolds number of $Re \approx 1$, to $C_{\rm D} \approx 0.5$ for $Re > 1000$ (e.g. Crowe et al. 1998). This suggests that filaments are more easily generated in flows with a low effective Reynolds number, which may be the case for the rarefied ICM. Despite these uncertainties, equation (11) remains informative because it indicates the functional relationship between physical parameters.

The observational quantities are slightly better constrained. In classical cool-core clusters, the entropy profile scales roughly linearly with distance all the way to the cluster centre (e.g. Sanderson et al. 2009), with a logarithmic gradient close to unity. We also assume the empirical relation that the bubble radius is linearly proportional to its displacement from the cluster centre, such that $r/z \sim 0.3 - 0.5$ (e.g. Diehl et al. 2008; McNamara & Nulsen 2007). Combining these values gives $L_{\rm buoy}/L_{\rm O} \sim 1 - 3$, indicating that material can potentially be displaced upwardly behind the bubble. Some of this material will come from the centre of the cluster and will be cool, meaning that an optical filament could form behind the rising bubble. Interestingly, Sanderson et al. (2009) present entropy profiles for a sample clusters, of which at least A1795, A2199 and A478 are nearly linear entropy profiles and also show evidence for filamentary structures (see Pope et al. 2008, and references therein). We also note that the typical mass in observed filaments of $\sim 10^8$ M$_\odot$ (e.g Salomé et al. 2008) agrees well with drift mass estimates for typical ICM bubbles. Additionally, the closeness of $L_{\rm buoy}/L_{\rm O}$ to unity in clusters with nearly linear entropy profiles also suggests that buoyant bubbles in these systems do not generate gravity waves, though powerful long-lived episodes of jet activity might (see, for example Omma et al. 2004).

Classical cool core clusters, however, comprise only a small fraction of the clusters. In general, cluster entropy profiles tend to flatten close to the centre and then increase roughly linearly with distance from the cluster centre (e.g. Donahue et al. 2006). If the entropy profile has a flat core when the bubble begins to rise (as opposed to being initially nearly linear and subsequently evolving into a cored profile due to the resulting heat injection), the logarithmic entropy gradient is approximately zero close to the cluster centre (see equation 8) and then roughly constant with a value near unity further out, e.g. 1.0-1.3 (e.g. Donahue et al. 2006; Cavagnolo et al. 2009). In this case, $L_{\rm buoy}/L_{\rm O}$ will be small near the cluster centre and the bubble motion will primarily generate turbulence which heats the central regions. Outside the central core, $L_{\rm buoy}/L_{\rm O}$ will take a value similar to that quoted above for the classical cool-core clusters and some material may be displaced upwards by the bubble. However, since the upward displacement can only occur outside the central entropy core, there is unlikely to be a significant amount of cool material in the drift region. In this case, the drift will likely not appear as optical filaments.

## 4 WAKE TRANSPORT

Apart from the drift, a rising bubble can also transport material via "wake transport". When a deformable bubble starts to rise, it takes on a shape that is roughly spherical, but with an indentation at the bottom. This cavity between a true sphere and the actual bubble shape with an indented base is known as the wake (e.g. Crowe 2005; Yang 2003; Schetz & Fuhs 1999). Figure 1 depicts a schematic view of the bubble, wake and drift. The "wake" in the present context is very different from the the turbulent wake that develops behind objects at high Reynolds numbers.

Studies of bubbles and mass transport by bubbles in non-cosmological settings indicate that line vortices generated behind the bubble as it begin to rise lift, trap the ambient medium in the vicinity (i.e. material in the cluster centre) within the "wake" cavity (c.f. Pavlovski et al. 2007). This trapped material is then carried up by the bubble.

In the first instance, material in the wake increases the average density of the bubble and as a direct consequence reduces its ascent velocity and the maximum height to which the bubble rises. In addition, trapped material can also drop out of the wake, and this material will further contribute to the formation of filaments behind AGN-blown bubbles.

### 4.1 Wake: a conceptual outline

Studies of fluidised beds indicate that a typical wake contains a fraction $q$ of the initial mass displaced by the bubble:

$$M_{\rm wake} \approx q M_{\rm dis,0}, \tag{12}$$

where $q \approx 0.24$ and $M_{\rm dis,0}$ is given by equation (4). Assuming that this laboratory value of $q$ is applicable to the intra-cluster medium, the above relationship suggests that AGN-inflated can easily lift few $\times 10^7$ to $\sim 10^8$ M$_\odot$ in their wakes.

In addition to facilitating the transport of material out of the cluster centre, the wake — and specifically, the mass in the wake — increases the effective average density of the bubble (though it does not affect the bubble's actual density contrast as measured from X-rays). As we discuss below, this modification impacts not only the maximum height that the bubble can ascend to, but also the efficiency with which energy is extracted from it.

We do, however, note that as in the case of the geometric constant $k$ in the estimate for the drift mass, we acknowledge an uncertainty: it is unclear whether the laboratory value of $q$ is applicable to the intra-cluster medium. It is difficult to propose a better motivated value because our understanding of the ICM microphysics is highly incomplete. This also means that the estimates of $q$ based on numerical simulations are not necessarily more believable than the laboratory value deduced from the observations of fluidised beds. On the other hand, one would expect that $q$ does not exceed unity, since this would imply that the wake contains more mass than originally displaced by the bubble; consequently, unless $q \ll 1$ for the ICM, our estimates for the wake mass in the range of $\sim 10^8$ M$_\odot$ should be reasonable.

### 4.2 The implications of wake transport

Studies of bubbles indicate that during the ascent, the bubble wake can lose blobs of material (Crowe 2005). Formally, this happens if the terminal infall velocity of a blob exceeds the local upward velocity behind the bubble. Once detached from the wake, the subsequent evolution of the material is unclear. In the simplest picture, the blob simple falls back inward. The presence of the ICM complicates the scenario in that the associated ram pressure will likely strip and stretch the blob into filamentary structures. Moreover, the material from the shredded blobs may also get caught in the drift behind the bubble and some of this material may still get displaced to larger distances from the cluster centre (Crowe 2005; Yang 2003).

This discussion would suggest that both drift and leakage of material from the bubble wake can contribute to the

formation of trailing filaments. However, the bulk of the wake material will tend to fall towards the cluster centre. As a result, the trailing material is unlikely to exhibit a single characteristic kinematic signature. Rather, the kinematic structure will depend on the relative importance of drift and leakage from the wake, and will probably vary significantly over time as different processes become prevalent. This issue bears further investigation.

As already noted, both the wake and drift affect the dynamics of the bubble, but in slightly different ways. To illustrate this, the equation of motion of a bubble carrying a wake, and subject to the action of drift, can be written as

$$\frac{\mathrm{d}[(M_{\rm bub}+M_{\rm wake}+M_{\rm drift})w]}{\mathrm{d}t} = g(M_{\rm bub}+M_{\rm wake}-M_{\rm dis})-F, \tag{13}$$

where $M_{\rm dis}$ is the mass displaced by the bubble, which falls with time, and $F$ is the drag force

$$F=\frac{1}{2}C_{\rm D}A\rho_{\rm ICM}w^2 \tag{14}$$

and $A=\pi r^2$ is the cross-sectional area of the spherical bubble.

From the left hand side of equation (13) it can be seen that a bubble of constant mass, $M_{\rm bub}$, which transports the additional masses, $M_{\rm wake}+M_{\rm drift}$, accelerates as if it has a larger effective mass of $M_{\rm bub}+M_{\rm wake}+M_{\rm drift}$. However, in the limit that the acceleration is zero, the bubble behaves slightly differently again; the terminal velocity of the bubble described by equation (13), can be expressed as

$$w_{\rm terminal}=\left[\frac{8}{3}\frac{gr}{C_{\rm D}}\left(1-\frac{M_{\rm wake}+M_{\rm bub}}{M_{\rm dis}}\right)\right]^{\frac{1}{2}}. \tag{15}$$

Equation (15) can be interpreted as the terminal velocity of a bubble with an effective density contrast of

$$\eta_{\rm eff}=\frac{M_{\rm dis}}{M_{\rm wake}+M_{\rm bub}}. \tag{16}$$

Denoting the effective density contrast when the bubble first starts to rise after inflation as $\eta_{\rm eff,0}$, we note that

$$\eta_{\rm eff,0}=\frac{\eta_0}{q\eta_0+1}, \tag{17}$$

where $\eta_0\equiv\rho_0/\rho_{\rm bub,0}=M_{\rm dis,0}/M_{\rm bub}$ is the *actual* initial density contrast and $M_{\rm dis,0}=\rho_0 V_0$ is the initial displaced mass. Here, $\rho_0$ is the ICM density where the bubble is inflated, and $\rho_{\rm bub,0}$, $V_0$ are the bubble mass density and the bubble volume once the bubble is inflated. A typical value of the actual initial density contrast taken from the literature is $\eta_0\sim 100$ (e.g. Ghizzardi et al. 2004). With mass in the wake characterized by $q\approx 0.24$ (see Yang 2003), $\eta_{\rm eff,0}\approx 4$. In this derivation, we have assumed that the mass of the bubble remains constant during the rise. This is equivalent to assuming that regardless of whether the ICM is entrained within the bubble at formation, the bubble does will not subsequently entrain any additional material during the rise. We have also assumed that the wake mass remains constant. The displaced mass is allowed to change since both the bubble volume and the ambient density vary with distance from the cluster centre and for completeness, we note that this mass will decrease as the bubble rises.

According to equation (15), the low effective density contrast reduces the terminal velocity of the bubble. In the initial stages, $\eta_{\rm eff,0}\approx 4$, results in a lower terminal velocity by a factor of $\sim 0.9$. And even though the effect is not large, it is worth bearing in mind since the bubble rise timescale, a quantity commonly used to estimate AGN power, is inversely proportionate to the velocity.

A lower density contrast also reduces the equilibrium height to which the bubble can rise and a sufficiently low contrast can result in the bubble not being able to rise beyond the very central regions of the cluster. This can be illustrated as follows.

Under the simplest circumstances, and ignoring fluid instabilities, the buoyant bubble will rise through the stratified atmosphere and expand adiabatically to maintain pressure equilibrium with its surroundings. Consequently, the bubble density can be related to the ambient density and temperature by (see also Hinton et al. 2007)

$$\frac{\rho_{\rm bub}}{\rho_{\rm bub,0}}=\left(\frac{\rho_{\rm ICM}}{\rho_0}\right)^{\frac{1}{\Gamma_{\rm b}}}\left(\frac{T_{\rm ICM}}{T_0}\right)^{\frac{1}{\Gamma_{\rm b}}}, \tag{18}$$

where $T_0$ and $\rho_0$ are the ICM temperature and density, respectively, where the bubble was inflated, $T_{\rm ICM}$ and $\rho_{\rm ICM}$ are the ambient temperature and density at the bubble's current location.

This relationship shows that the bubble density drops more slowly than the ambient density and there will be a location where the densities become comparable. In the absence of a wake, the buoyancy force would also vanish at this height, and the upward motion of the bubble would stagnate since this motion is driven by buoyancy. In practice, due to the kinetic energy gained by the bubble, it will not immediately come to halt at the equilibrium height. Instead, it will overshoot this location. Above the equilibrium height, the bubble will be denser than its surroundings and experience a gravitational restoring force towards the cluster centre. Consequently, it will oscillate around the equilibrium radius at approximately the Brunt-Väisälä (buoyancy) frequency (e.g. Choudhuri 1998). The oscillation will, in due course, be damped by the drag force but while it is oscillating, the bubble will generate fluid disturbances that travel towards and away from the cluster centre. Consequently, a fraction of the kinetic energy gained during the ascent can go towards heating the central regions of the ICM.

The arresting criterion for the bubble-wake system, in the presence of the wake, is obtained from equation (13) by noting that at the equilibrium height, $z_{\rm eq}$

$$M_{\rm wake}(z_{\rm eq})\approx M_{\rm dis}(z_{\rm eq})-M_{\rm bub}, \tag{19}$$

where $M_{\rm dis}(z_{\rm eq})=\rho_{\rm ICM}(z_{\rm eq})V_{\rm bub}(z_{\rm eq})$ is the displaced mass at the equilibrium location. This criterion is equivalent to $\eta_{\rm eff}(z_{\rm eq})=1$.

Since $\eta_{\rm eff}$ can be written as

$$\eta_{\rm eff}=\eta_{\rm eff,0}\left(\frac{\rho_{\rm ICM}}{\rho_0}\right)^{\frac{\Gamma_{\rm b}-1}{\Gamma_{\rm b}}}\left(\frac{T_{\rm ICM}}{T_0}\right)^{\frac{-1}{\Gamma_{\rm b}}}, \tag{20}$$

then $\eta_{\rm eff}(z_{\rm eq})=1$ at the equilibrium height implies,

$$\frac{\rho_{\rm ICM}(z_{\rm eq})}{\rho_0}=\eta_{\rm eff,0}^{-\frac{\Gamma_{\rm b}}{\Gamma_{\rm b}-1}}\left[\frac{T_{\rm ICM}(z_{\rm eq})}{T_0}\right]^{\frac{1}{\Gamma_{\rm b}-1}}. \tag{21}$$

where $T_{\rm ICM}(z_{\rm eq})$ is the ICM temperature at the equilibrium height. For cool-core clusters we typically expect $T_{\rm ICM}(z_{\rm eq})/T_0\sim 3$ (e.g. Allen et al. 2001).

Modelling the ICM density distribution using a $\beta$-profile

$$\rho_{\rm ICM}(z) = \rho_{\rm ICM,0}\left[1+\left(\frac{z}{z_{\rm ICM,0}}\right)^2\right]^{-\beta}, \qquad (22)$$

where $\rho_{\rm ICM,0}$ is the central ICM density, $z_{\rm ICM,0}$ is the ICM scale height, and $z$ is the distance from the cluster centre, we can estimate the equilibrium height to which an adiabatic buoyant bubble carrying a wake, inflated at height $z_0$, will rise in such an atmosphere:

$$\left(\frac{z_{\rm eq}}{z_0}\right)^2 = \left[1+\left(\frac{z_{\rm ICM,0}}{z_0}\right)^2\right] \times \eta_{\rm eff,0}^{\frac{\Gamma_{\rm b}}{\beta(\Gamma_{\rm b}-1)}}\left[\frac{T_{\rm ICM}(z_{\rm eq})}{T_0}\right]^{-\frac{1}{\beta(\Gamma_{\rm b}-1)}} - \left(\frac{z_{\rm ICM,0}}{z_0}\right)^2 \qquad (23)$$

Restricting ourselves to classical cool core clusters that generically exhibit very small scale heights and hence, nearly power-law density profiles, we find that

$$\left(\frac{z_{\rm eq}}{z_0}\right)^2 \approx \eta_{\rm eff,0}^{\frac{\Gamma_{\rm b}}{\beta(\Gamma_{\rm b}-1)}}\left[\frac{T_{\rm ICM}(z_{\rm eq})}{T_0}\right]^{-\frac{1}{\beta(\Gamma_{\rm b}-1)}} \qquad (24)$$

In Figure 2, we plot equation (24) as a function of $q \equiv M_{\rm wake}/M_{\rm dis,0}$ for three different values of the initial density contrast $\eta_{\rm eff,0} = 1000, 100, 10, 4$, assuming $\Gamma_{\rm b} = 4/3$, $\beta = 3/4$ and $T_{\rm ICM}(z_{\rm eq})/T_0 = 3$ (as is appropriate in cool core clusters).

It can be seen that a low effective density contrast due to the wake can significantly affect the equilibrium height, resulting in the bubble being trapped closer to the cluster centre. Specifically, we find that if we ignore the wake (i.e. set $q = 0$), then $\eta_{\rm eff,0} = \eta_0 \approx 100$ and $z_{\rm eq} \sim$ few $\times\, 10^3 z_0$, which probably greatly exceeds the cluster virial radius even if $z_0$ is small (i.e. $z_0 \approx 1$—$30\,$kpc). For the same situation, if $q = 0.24$ and $\eta_0 = 100$, then $\eta_{\rm eff,0} \approx 4$ and $z_{\rm eq} \sim 4.5 z_0$. If the bubble is inflated and begins its ascent from $z_0 = 10\,$kpc, it will arrest at $\sim 50$ kpc.

For completeness, we note that the ratio of the final to initial pressure is

$$\frac{P(z_{\rm eq})}{P_0} = \left[\eta_{\rm eff,0}\frac{T_0}{T_{\rm ICM}(z_{\rm eq})}\right]^{-\frac{\Gamma_{\rm b}}{\Gamma_{\rm b}-1}}. \qquad (25)$$

It can also be shown that the bubble's density contrast is important for governing the efficiency with which energy is extracted. The total energy available for heating the ICM and transporting mass is obtained by integrating the buoyancy force acting on the bubble along its path of motion (c.f. Churazov et al. 2002; Nusser et al. 2006)

$$\int_{z_0}^{z_{\rm eq}} F_{\rm buoy}{\rm d}z = \int_{z_0}^{z_{\rm eq}} V_{\rm bub}\rho_{\rm bub} g{\rm d}z - \int_{z_0}^{z_{\rm eq}} V_{\rm bub}\rho_{\rm ICM} g{\rm d}z + \int_{z_0}^{z_{\rm eq}} M_{\rm wake} g{\rm d}z \qquad (26)$$

where $g$ is the gravitational acceleration. Making use of the fact that the ICM is in hydrostatic equilibrium, the second term on the right hand side of equation (26) can be rewritten as

$$V_{\rm bub}\rho_{\rm ICM} g{\rm d}z \approx V_{\rm bub}\frac{{\rm d}P}{{\rm d}z}{\rm d}z = V_{\rm bub}{\rm d}P, \qquad (27)$$

where $P$ is both the pressure in the bubble and the ICM pressure. These two are assumed to be equal since the bubble is in pressure equilibrium with its surroundings. Using equation (25) and the fact that the bubble expands adiabatically,

$$\int_{P_0}^{P(z_{\rm eq})} V_{\rm bub}{\rm d}P = \frac{\Gamma_{\rm b}}{(\Gamma_{\rm b}-1)}P_0 V_0\left[\left(\frac{T_{\rm ICM}(z_{\rm eq})}{\eta_{\rm eff,0}T_0}\right)-1\right], \qquad (28)$$

where we have used equation (25) to derive the latter relationship.

The remaining two terms on the right side of equation (26) can also be approximated if we make some reasonable assumptions about the bubble-wake-ICM system. For example, for a bubble-wake system where $M_{\rm bub} + M_{\rm wake}$ is constant, the requirement that the ICM is in hydrostatic equilibrium allows us to write

$$\int_{z_0}^{z_{\rm eq}} V_{\rm bub}\rho_{\rm bub}\, g{\rm d}z + \int_{z_0}^{z_{\rm eq}} M_{\rm wake}\, g{\rm d}z \approx \frac{M_{\rm dis,0}}{\eta_{\rm eff,0}}\int_{P_0}^{P(z_{\rm eq})}\frac{{\rm d}P}{\rho_{\rm ICM}}. \qquad (29)$$

To make further progress, we restrict ourselves to classical cool core clusters whose entropy profiles scale nearly linearly with distance from the cluster centre (e.g. Sanderson et al. 2009) and in keeping the observations, we approximate that the ICM density profile for classical cool core clusters as a power-law: $\rho_{\rm ICM} \approx \rho_0\,(z/z_0)^{-2\beta}$. This profile is equivalent to the $\beta$-profile in equation (22) in the limit $z_0 \gg z_{\rm ICM,0}$, where $z_0$ is the radius at which the bubble is inflated. For $\beta = 3/4$, we find that

$$\int_{z_0}^{z_{\rm eq}} V_{\rm bub}\rho_{\rm bub}\, g{\rm d}z + \int_{z_0}^{z_{\rm eq}} M_{\rm wake}\, g{\rm d}z \approx \frac{\Gamma_{\rm b}}{(\Gamma_{\rm b}-1)}\frac{P_0 V_0}{\eta_{\rm eff,0}}\ln\left(\frac{T_{\rm ICM}(z_{\rm eq})}{\eta_{\rm eff,0}T_0}\right), \qquad (30)$$

where we have applied equation (25).

Combining equations (28) and (30), we find that

$$\int_{z_0}^{z_{\rm eq}} F_{\rm buoy}{\rm d}z \approx \frac{\Gamma_{\rm b}}{(\Gamma_{\rm b}-1)}P_0 V_0 \times\left[1+\frac{1}{\eta_{\rm eff,0}}\ln\left(\frac{T_{\rm ICM}(z_{\rm eq})}{\eta_{\rm eff,0}T_0}\right)-\left(\frac{T_{\rm ICM}(z_{\rm eq})}{\eta_{\rm eff,0}T_0}\right)\right]. \qquad (31)$$

For $T_{\rm ICM}(z_{\rm eq})/T_0 \approx 3$, comparing the energy available for heating when $\eta_{\rm eff,0} \approx 100$ and $\eta_{\rm eff,0} \approx 4$, which is the more appropriate value when the wake mass is taken into account and corresponds to $q \approx 0.24$, we find that heating is reduced by a factor of $\sim 6$ in the latter case. Physically, this means that some of the bubble's energy goes into raising the potential energy of its content, including the wake, and is therefore unavailable for heating the ICM. The lower the density contrast between the bubble and its surroundings, the lower the fraction of energy released during the ascent.

## 5 ENTRAINMENT

Mass transport may also proceed by the entrainment of ICM material into the bubble — the drawing-in and incorporation of material from the ICM into the bubble body — and its subsequent displacement to larger radii in the cluster, as the bubble rises (c.f. McCarthy et al. 2008).

Entrainment can impact bubble dynamics in two important ways: (1) It causes the bubble to expand more rapidly

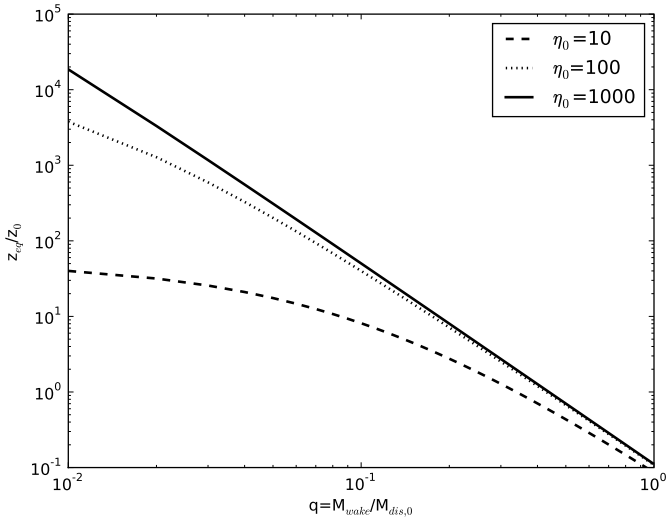


**Figure 2.** Plot showing the equilibrium height as a function of $q = M_{\rm wake}/M_{\rm dis,0}$, for three values of $\eta_0$ using equation (24). For this plot, $\Gamma_{\rm b} = 4/3$, $\beta = 3/4$ and $T_{\rm ICM}(z_{\rm eq})/T_0 = 3$.

than predicted by a simple adiabatic model, and (2) it limits the height to which a bubble can rise. The importance of this particular channel, however, depends on the extent to which material is drawn into the bubble.

Establishing the extent of entrainment in AGN-inflated bubbles is a non-trivial task. Entrainment is an extremely complex phenomenon and can occur in several ways. For example, the ambient material may not be displaced by the jet with 100% efficiency, resulting in the entrainment of some ICM material within the bubble. Kelvin-Helmholtz instabilities due to shear between the jet and the ICM can also draw ambient material in through the sides of the jet. Additionally, Rayleigh-Taylor instabilities on the upper bubble surface can allow the ICM material to penetrate, resulting in a time-varying mass entrainment rate as the bubble rises. On the other hand, given that the observed bubbles appear to be highly resilient to instabilities that can transform spherical bubbles into vortex rings, a number of researchers have suggested that the AGN-blown bubbles may either be draped by surface magnetic fields, or that the ICM may be more viscous than thought (e.g. De Young 2003; Kaiser et al. 2005). Both surface magnetic fields and enhanced ICM viscosity dramatically inhibit mixing and the growth of fluid instabilities. But even in these situations, intra-cluster material can still enter the bubble. For example, in the case of a bubble surface draped by surface magnetic fields, the ICM can still leak into the bubble as a consequence of magnetic reconnection events and diffusion across the bubble/ICM boundary, (see Pope 2010).

The upshot here is that entrainment of the ICM into AGN-blown bubbles is not governed by hydrodynamic processes alone. As a result, findings from current generation of numerical hydrodynamic (and even magnetohydrodynamic) simulations are not directly applicable; these do not, as of yet, adequately capture the necessary microphysical processes. This then argues in favour of treating the process in a more general manner, as we attempt to do here, with explicit (rather than implicit) assumptions about the nature of the fluid flow.

### 5.1 Entrainment: a conceptual overview

As a starting point, we turn to the conservation equations for mass, momentum and thermal energy that are often applied to the study of plumes in the terrestrial atmosphere (e.g. Turner 1969). In doing so, we avoid having to make any implicit assumptions about the fluid behaviour of the ICM, in contrast to standard hydrodynamic simulations. For example, the flow of an inviscid, rarefied fluid around an obstacle can have a low effective Reynolds number (e.g. Shen 2005), which cannot be accounted for in the continuous fluid approximation. Furthermore, the Reynolds number range accessible to hydrodynamic simulations is $Re \lesssim n^2$, where $n$ is the number of computational cells across the width of the flow. Consequently, coarser spatial resolution implies a larger effective viscosity that may act to reduce the growth rate of instabilities on the bubble surface, which affects the entrainment rate. Instead, we model the effective Reynolds number of the flow, affected by rarefication and viscosity, through the drag and entrainment coefficients. In particular, the drag coefficient is related to the Reynolds number (e.g. see Pope et al. 2008, for an approximate functional form) and hence the effective viscosity. Furthermore, we calibrate the entrainment rate to match mixing rates due to the growth of Rayleigh-Taylor instabilities in hydrodynamic simulations of buoyant bubbles in cluster atmospheres (e.g. Churazov et al. 2001; Pavlovski et al. 2008). Applicability to the ICM is also extended by accounting for the different adiabatic indices of the bubble and the ICM.

Integrating the equations then yields the bubble radius, velocity and density as it evolves in an external medium. Importantly, since the bubble is assumed to be spherically symmetric, the integration can be performed to very high precision so that numerical errors are significantly diminished. It is also staightforward to ensure the equations are

entirely self-consistent and that the appropriate quantities are conserved.

Nevertheless, certain assumptions are required to solve the conservation equations given below; the most important being that the bubble remains spherical, intact and in pressure equilibrium with its surroundings. This is observationally justifiable; with the possible exception of M87 which appears to exhibit a vortex ring structure (Owen et al. 2000). The ICM is also taken to be hydrostatic and we omit any effects due to radiative processes and thermal conductivity. Other than this, the derivation does not make any assumptions about the shape of the ICM density or temperature profiles.These assumptions are similar to many numerical simulations of bubbles and are permissible for the following reasons. Radiative losses from the bubble depend on its particle content, which is difficult to determine and might plausibly be small. Thermal conduction of heat across the bubble/ICM must be strongly suppressed, probably by magnetic fields, otherwise bubbles would rapidly evaporate (Pavlovski et al. 2008).

To make the model as transparent as possible, we have employed the well-known entrainment hypothesis which states that the velocity, $v$, at which material joins the bubble is proportional to the ascent velocity of the bubble, $w$ (Turner 1969). The constant of proportionality, $\alpha$, is called the entrainment coefficient and is defined by

$$v = \alpha w. \tag{32}$$

In a uniform medium, and in the Boussinesq limit, the typical entrainment coefficient for a momentum-driven outflow is $\alpha \sim 0.05$ and $\sim 0.08$ for a buoyancy-driven flow (e.g. Turner 1986). De Young (2006) also describes how the entrainment coefficient may vary with the density contrast, $\eta$, and Mach number, $Ma$, such that $\alpha \sim 0.2(Ma/0.5)^{-1}(\eta/2)^{1/2}$. However, this functional form is representative of mixing due to non-linear Kelvin-Helmholtz instabilites, which are suppressed on the surface of a magnetised AGN-blown bubble. As a result, we assume $\alpha$ to be a constant.

Following equation (32), the equation of mass conservation for an entraining bubble is

$$\frac{\mathrm{d}M_{\rm bub}}{\mathrm{d}t} = \alpha a_{\rm bub}\rho_{\rm ICM} w, \tag{33}$$

where $a_{\rm b}$ is the surface area of the bubble. The relation is best expressed in terms of the distance from the cluster centre, so, assuming that $\frac{\mathrm{d}}{\mathrm{d}t} = w\frac{\mathrm{d}}{\mathrm{d}z}$ and the bubble is spherical, we can write

$$\frac{\mathrm{d}M_{\rm bub}}{\mathrm{d}z} = 4\pi r^2 \alpha \rho_{\rm ICM}. \tag{34}$$

Substituting $M_{\rm bub} = \rho_{\rm bub}V_{\rm bub}$ into equation (34) gives

$$\frac{\mathrm{d}r}{\mathrm{d}z} = \alpha\frac{\rho_{\rm ICM}}{\rho_{\rm bub}} - \frac{r}{3}\frac{1}{\rho_{\rm bub}}\frac{\mathrm{d}\rho_{\rm bub}}{\mathrm{d}z}. \tag{35}$$

Using equation (35), forms the basis for calibrating $\alpha$ against numerical simulations of bubbles in cluster atmospheres. The length scale over which entrainment dominates the mass of the bubble can be defined as the distance, $L$, during which the bubble entrains a mass comparable to the initial displaced mass. To first order, the entrainment length is given by

$$L \equiv \left(\frac{1}{M_{\rm dis,0}}\frac{\mathrm{d}M_{\rm bub}}{\mathrm{d}z}\right)^{-1} \sim 11\left(\frac{r_0}{5\,\mathrm{kpc}}\right)\left(\frac{\alpha}{0.15}\right)^{-1}\,\mathrm{kpc} \tag{36}$$

where $r_0$ is the initial bubble radius. [2] Hydrodynamic simulations of bubbles in galaxy clusters show that bubbles almost completely mix with their surroundings before they have ascended a distance of roughly 2-3 initial bubble radii (e.g. Churazov et al. 2001; Robinson et al. 2004; Gardini 2007; Pavlovski et al. 2008). On this evidence, the effective entrainment coefficient due to the development of Rayleigh-Taylor instabilities must be $\alpha \sim 0.1 - 0.15$. The effect of viscosity and magnetic fields are equivalent to a reduction of $\alpha$.

To proceed further, it is necessary to consider the momentum and thermal energy equations. The momentum equation is given by equation (13) using $k\rho_{\rm ICM}V_{\rm bub} = M_{\rm drift}$ and a constant wake mass of $qM_{\rm dis,0}$. The thermal energy equation can be derived from the following statement: the addition of a mass of gas, $\mathrm{d}M_{\rm bub}$, at temperature $T_{\rm ICM}$, and at constant pressure, changes the internal energy of the bubble, $c_{\rm p,bub}T_{\rm bub}M_{\rm bub}$. In this description, $c_{\rm p,bub}$ is the specific heat capacity at constant pressure, per unit mass of the bubble and $c_{\rm p,bub} = \Gamma_{\rm b}k_{\rm B}/[\mu m_{\rm p}(\Gamma_{\rm b}-1)]$, where $\Gamma_{\rm b}$ is the adiabatic index of the bubble material. The thermal energy equation is then

$$\begin{aligned} &c_{\rm p,ICM}T_{\rm ICM}\mathrm{d}M_{\rm bub} + c_{\rm p,bub}T_{\rm bub}M_{\rm bub} = \\ &(T_{\rm bub}+\mathrm{d}T_{\rm bub})(M_{\rm bub}+\mathrm{d}M_{\rm bub})c_{\rm p,bub}, \end{aligned} \tag{37}$$

where $c_{\rm p,ICM} = \Gamma_{\rm ICM}k_{\rm B}/[\mu m_{\rm p}(\Gamma_{\rm ICM}-1)]$, is the specific heat at constant pressure per unit mass of the ambient gas.

Expanding the right hand side of equation (37) up to first order terms and rearranging gives

$$\frac{\mathrm{d}\rho_{\rm bub}}{\rho_{\rm bub}} = \frac{\mathrm{d}M_{\rm bub}}{M_{\rm bub}}\left[1 - \frac{\Gamma_{\rm ICM}(\Gamma_{\rm b}-1)}{\Gamma_{\rm b}(\Gamma_{\rm ICM}-1)}\frac{\rho_{\rm bub}}{\rho_{\rm ICM}}\right]. \tag{38}$$

The density of the bubble is also affected by adiabatic expansion. Assuming the atmosphere is hydrostatic, the change in density can be written in terms of the gravitational acceleration of the cluster

$$\frac{\mathrm{d}\rho_{\rm bub}}{\rho_{\rm bub}} = \frac{\mathrm{d}P}{\Gamma_{\rm b}P} = \frac{\mu m_{\rm p} g \mathrm{d}z}{\Gamma_{\rm b}k_{\rm B}T_{\rm ICM}}. \tag{39}$$

However, because the bubble now contains a mixture of fluids with different adiabatic indices, its expansion must be described in terms of a single, time-dependent effective adiabatic index calculated in the following way. Entraining a mass of material, $\Delta M$, at the same pressure, is equivalent to entraining a volume $\Delta V = \Delta M/\rho_{\rm ICM}$. This increases the internal energy of the bubble by an amount $P\Delta V/(\Gamma_{\rm ICM}-1)$, after which the total must be

$$\frac{P(V_{\rm bub}+\Delta V)}{\Gamma - 1} = P\left[\frac{V_{\rm bub}}{\Gamma_{\rm b}-1} + \frac{\Delta V}{\Gamma_{\rm ICM}-1}\right], \tag{40}$$

where $\Gamma$ is the effective adiabatic index. Then, after the $i$th

[2] The critical value of $\alpha$ above which equation (36) strictly holds occurs for $L = z_{ICM,0}$, so that $\alpha_{\rm crit} = r_0/(3z_{ICM,0})$. For the current setup with an initial bubble size of $r_0 = 5$ kpc, and a density scale height of $z_{ICM,0} = 18.6$ kpc, we find $\alpha_{\rm crit} \approx 0.09$.

timestep of the numerical integration, the updated value of $\Gamma$ must be

$$\frac{1}{\Gamma_{\rm i+1}-1}=\frac{1}{(V_{\rm i}+\Delta V_{\rm i})}\left[\frac{V_{\rm i}}{\Gamma_{\rm i}-1}+\frac{\Delta V_{\rm i}}{\Gamma_{\rm ICM}-1}\right], \qquad (41)$$

where $\Delta V_{\rm i}$ is entrained volume during the $i$th timestep, so that $V_{\rm i}+\Delta V_{\rm i}$ is the total bubble volume after the timestep, $\Gamma_{\rm i}$ was the effective adiabatic index at the beginning of the timestep and $\Gamma_{\rm ICM}$ is the adiabatic index of the ICM. In the subsequent equations and numerical calculations we use $\Gamma_{\rm b}=\Gamma_{\rm i}$.

Equations (35), (13), (38) and (39) can then be rearranged to yield simultaneous differential equations for the bubble radius, density and velocity

$$\frac{{\rm d}r}{{\rm d}z}=\alpha\frac{\Gamma_{\rm ICM}}{\Gamma_{\rm b}}\frac{(\Gamma_{\rm b}-1)}{(\Gamma_{\rm ICM}-1)}-\frac{\mu m_{\rm p} r g}{3\Gamma_{\rm b}k_{\rm B}T_{\rm ICM}}, \qquad (42)$$

$$\frac{{\rm d}\rho_{\rm bub}}{{\rm d}z}=\frac{3\alpha}{r}\left[\rho_{\rm ICM}-\frac{\Gamma_{\rm ICM}}{\Gamma_{\rm b}}\frac{(\Gamma_{\rm b}-1)}{(\Gamma_{\rm ICM}-1)}\rho_{\rm bub}\right]+\frac{\mu m_{\rm p}\rho_{\rm bub}g}{\Gamma_{\rm b}k_{\rm B}T_{\rm ICM}}, \qquad (43)$$

and

$$\begin{aligned}\frac{{\rm d}w}{{\rm d}z}=&\frac{-3\alpha w\rho_{\rm ICM}/r}{\rho_{\rm tot}}\left[1+\frac{\Gamma_{\rm ICM}}{\Gamma_{\rm b}}\frac{(\Gamma_{\rm b}-1)}{(\Gamma_{\rm ICM}-1)}\right]\\&+\frac{g}{w}\frac{(\rho_{\rm tot}-(1+k)\rho_{\rm ICM})}{\rho_{\rm tot}}\\&-\frac{(\Gamma_{\rm b}-1)\mu m_{\rm p}wg}{\Gamma_{\rm b}k_{\rm B}T_{\rm ICM}}\frac{k\rho_{\rm ICM}}{\rho_{\rm tot}}\\&-\frac{F}{V_{\rm bub}w\rho_{\rm tot}}.\end{aligned} \qquad (44)$$

where $V_{\rm bub}$ is the bubble volume, $k\rho_{\rm ICM}V_{\rm bub}$ is the drift mass and defining a total effective density

$$\rho_{\rm tot}\equiv\rho_{\rm bub}+k\rho_{\rm ICM}+\frac{qM_{\rm dis,0}}{V_{\rm bub}}, \qquad (45)$$

with $qM_{\rm dis,0}$ being the wake mass.

The terms in equation (44) represent entrainment, buoyancy, added mass and drag, respectively. A further brief inspection reveals that the adiabatic relations are recovered in the limit that entrainment is unimportant ($\alpha\rightarrow 0$). The effective adiabatic index of the fluid mixture within the bubble is given by equation (41).

In addition to these equations, we must also specify functional forms for the ICM density and temperature, which can be used to calculate the background gravitational field. As an example, the ICM density can be modelled as a $\beta$-profile, e.g. equation (22). For the temperature profile, we use the Gaussian function used by Ghizzardi et al. (2004) to describe the ICM temperature of the Virgo cluster

$$T_{\rm ICM}=T_1-T_2\exp\left(-\frac{1}{2}\frac{z^2}{z_{\rm T}^2}\right), \qquad (46)$$

where $T_1$ is the ICM temperature at large radii, and $T_1-T_2$ is the temperature in the centre of the cluster. $z_{\rm T}$ is the scale height of the temperature profile.

The background gravitational acceleration of the cluster potential is determined from the temperature and density profiles by assuming the gas is in hydrostatic equilibrium

$$g=\frac{k_{\rm B}}{\mu m_{\rm p}}\left(\frac{{\rm d}T_{\rm ICM}}{{\rm d}z}+\frac{T_{\rm ICM}}{\rho_{\rm ICM}}\frac{{\rm d}\rho_{\rm ICM}}{{\rm d}z}\right) \qquad (47)$$

Within this framework, we take a fit from Pope et al. (2006) to the density profile of the Hydra cluster based on the data given by David et al. (2001). The values are representative of general cluster density profiles and are $\rho_0=0.7\times10^{-25}\,{\rm g\,cm^{-3}}$, $\beta=0.72$ and $z_{\rm ICM,0}=18.6\,{\rm kpc}$. The temperature is taken to be a typical cool core cluster in which the central temperature is a factor of 3 lower than at large radii: $T_1=3\times10^7\,{\rm K}$, $T_2=2\times10^7\,{\rm K}$ with $z_{\rm T}=5.0\,{\rm kpc}$.

To illustrate the model, we have numerically integrated equations (42), (43) and (44) using a standard fourth-order Runge-Kutta method. For the initial conditions, the bubbles were placed 10 kpc from the cluster centre, with a radius of 5 kpc and a density contrast of $\approx 40$. In both entraining and non-entraining cases, the added mass coefficient was set to $k=0.5$, with $q=0.24$. The initial adiabatic index of the bubble is $\Gamma_{\rm b,0}=4/3$, $\Gamma_{\rm ICM}=5/3$ and $C_{\rm D}=0.5$. By definition, $\alpha=0$ in the non-entraining case, while for the entraining bubble we set $\alpha=0.15$, as expected for mixing due to Rayleigh-Taylor instabilities.

Figure 3 shows the density contrast of bubbles evolving in the Hydra-like cluster atmosphere. In these plots, the solid line represents the non-entraining bubble, while the long and short dashed lines indicate the behaviour of the entraining bubble with and without a wake, respectively.

As can be seen from figure 3, it is clear that entrainment increases the rate of expansion of the bubble over and above what would be expected due to adiabatic expansion. According to equation (42), for large values of $\alpha$ the half-opening angle of a bubble would tend to

$$\tan(\theta)\equiv\frac{{\rm d}r}{{\rm d}z}\sim\frac{5}{8}\alpha, \qquad (48)$$

using $\Gamma_{\rm b}=4/3$ and $\Gamma_{\rm ICM}=5/3$.

### 5.2 Entrainment: Observational implications

As already discussed in the context of the bubble wake, bubble dynamics and energetics both depend on the density contrast of a rising bubble. Entrainment obviously contributes to the lowering of this contrast. In addition to this, understanding the impact of entrainment is of particular interest because Diehl et al. (2008) have noted that bubble radii are approximately half their distance from the cluster centre. They argue that this correlation is too large and too constant to be attributable to simple adiabatic evolution. Diehl et al. (2008) favour a model where bubbles are inflated by current-dominated jet (Nakamura et al. 2006). Brüggen et al. (2009), however, argue that this behaviour may well be explicable by a combination of projection effects and modifying the standard adiabatic model to include the influence of entrainment.

According to observations, the typical opening angle of a bubble is roughly $\tan(\theta)\sim 0.5$, (e.g. Diehl et al. 2008). If entrainment is the physical process which leads to this, equation (48) implies that $\alpha\sim 0.8$. This, in turn, implies an entrainment length-scale of $L\sim r_0/2$. In other words, the bubble could only rise a distance equivalent to the initial bubble radius before it became indistinguishable from its surroundings. It is difficult to rule out this possibility entirely since we cannot know the bubble radii at earlier times. However, bubbles clearly persist out to large distances - the cavity statistics provided by Bîrzan et al. (2004) indicate

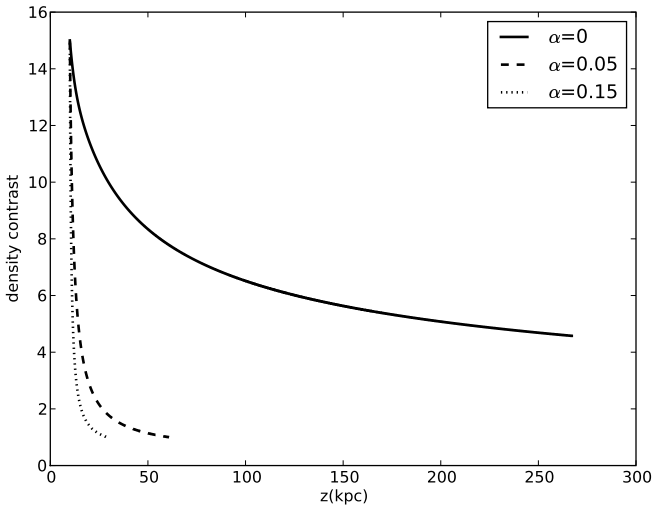


**Figure 3.** Plot showing the density contrast for the entraining bubble ($\alpha = 0.15, 0.05$) and a non-entraining bubble ($\alpha = 0$). Note that the density contrast rapidly becomes small in the entraining cases. In fact, the final density contrast is less than unity because $\Gamma_{\rm b}$ is always less than $\Gamma_{\rm ICM}$, see equation (43).

that there are bubbles located more than 20 kpc from the cluster centre in Perseus, A4059, A133, A2199, RBS 797, A2597, Hydra A, Cygnus A.

Moreover, Sanders & Fabian (2007) argue, based on an analysis of the bubbles in Perseus, that the volume fraction of thermal material in bubbles cannot exceed 50%. The conversion of the volume fraction into a mass fraction depends requires making certain assumptions about, for example, the temperature of the entrained material and whether it is heated significantly as it enters the bubble. Nonetheless, it is possible to derive some general expectations: if the entrained material is at the ambient temperature then the density contrast of the rising bubbles must be high and the entrainment process must be very inefficient (i.e. $\alpha$ must be small), otherwise the bubbles would not appear as depressions in the X-ray surface brightness maps(e.g. McNamara & Nulsen 2007). If the entrained gas is heated above 15 keV, it would be difficult to detect using existing X-ray telescopes and therefore, the appearance of AGN bubbles as depressions in the X-ray surface brightness maps offers no constraint. On the other hand, if the bubble and the ICM are in pressure equilibrium, then the fraction of the bubble mass attributed to entrainment depends roughly on the ratio of the ambient temperature to that of the newly heated material in the bubble (e.g. McCarthy et al. 2008). If the entrained material is heated significantly, the entrained mass can again not be very large. For example, if the entrained material is heated to be, say, five times the temperature of the ambient gas, the bubble will contain at most one fifth of the mass originally displaced by the inflation process.

Consequently, the upper limit of 50% for the volume fraction of the thermal content strongly suggests that the bubbles cannot be entraining rapidly and the large opening angles must have a different explanation. This can be illustrated using the similar reasoning used to derive equation (40). Specifically, the pressure fraction, $f_{\rm i+1}$, contributed by entrained material after the $i$th timestep of the numerical integration using

$$\frac{1}{\Gamma_{\rm i+1}-1} = \frac{1-f_{\rm i+1}}{\Gamma_{\rm b,0}-1} + \frac{f_{\rm i+1}}{\Gamma_{\rm ICM}-1}, \qquad (49)$$

where $\Gamma_{\rm b,0}$ is the initial adiabatic index of the bubble before it entrained any material from its surroundings and $f_{\rm i+1}$ = thermal pressure/total pressure. Note that this is the volume-averaged pressure fraction. Therefore, since the pressures of each component must have been equal, and given that material is entrained at constant pressure, the volume-averaged pressure fraction is equivalent to the volume fraction of thermal material.

Figure 4 clearly shows that, for $\alpha = 0.15$, the thermal pressure fraction grows rapidly to greater than 0.6 before the bubble has risen 10 kpc from its original location. However, for $\alpha = 0.05$, the pressure fraction is 0.5 at roughly 40 kpc from the cluster centre and rises much more slowly. For $\alpha = 0.01$, the pressure fraction remains <50% even beyond 150 kpc. Consequently, a thermal volume fraction of $\sim 50\%$ suggests either that the thermal content was injected (or entrained) during the initial inflation, or that the subsequent entrainment rate is no larger than $\alpha \approx 0.05$. This reduced rate probably indicates that magnetic fields at the bubble/ICM interface suppress the growth of fluid instabilities, while still permitting a small amount of thermal material to enter the bubble due to cross-field diffusion and magnetic reconnection events (e.g. Pope 2010). In any case, the large opening angles of the bubbles cannot be due to entrainment. Alternative possibilities include:
(1) The bubbles are hydrodynamic in origin and the apparently large opening angle is partially due to projection effects, as suggested by Brüggen et al. (2009);
(2) The bubbles are *not* hydrodynamic in nature and are formed by a different inflation process, e.g. current-dominated jets, as suggested by Diehl et al. (2008).

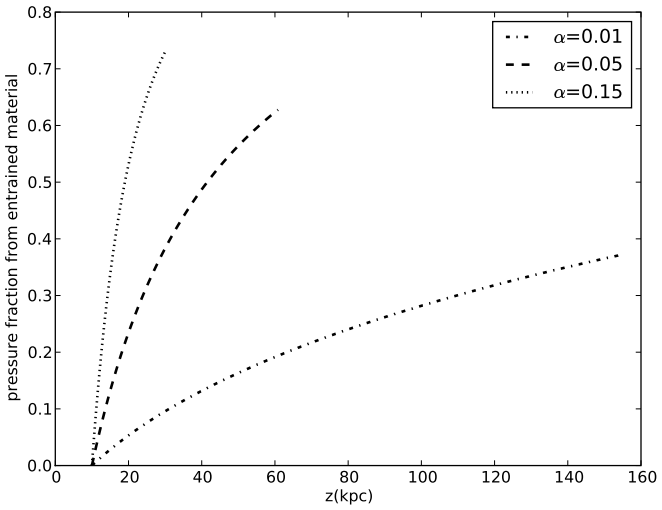


**Figure 4.** Plot showing the fraction of internal bubble pressure contributed by entrained material for different entrainment rates: $\alpha = 0.15, 0.05, 0.01$. By definition, the pressure fraction for the non-entraining bubble is always zero.

## 6 DISCUSSION

Having examined the three main mass transport processes associated with a buoyant bubble individually, we now consider the three processes jointly and ask:
(1) how much material in total can actually be transported per bubble?
(2) how frequently must bubbles be inflated in order for the mass outflow to balance the cooling inflow?

Regarding the first question, we have already established that the bubbles cannot be carrying very much entrained material. The drift can carry upward an amount of ambient material comparable to 50% of the mass initially displaced by the bubble, or approximately $\sim 10^8\,\mathrm{M}_\odot$. However, most of this material will not be displaced upwards by more than a bubble diameter and will likely fall back towards the cluster centre. In addition, for clusters with a flat entropy core, the overall fluid displacement might be negligible. This then means that the drift, though likely responsible for observable features like the cool optical filaments, is not an important mechanism for affecting mass outflow.

This leaves the wake. As noted previously, fluidised bed experiments (e.g. Yang 2003) show that wake typically contains a approximately a quarter of the mass initially displaced by the bubble. Assuming that laboratory value of $q$ can be applied to the ICM, AGN-blown bubble wakes could easily transport $qM_{\mathrm{dis},0} \sim 10^8\,\mathrm{M}_\odot$, see equation (4).

Moreover, the mass in the wake can be carried out to large distances. As indicated by equation (24), the maximum bubble height is a strong function of $q$. For $q \sim 0.24$ (and $\eta_0 = 100$), depending on the temperature profile, the bubble can rise to at least $5z_0$, where $z_0$ is the height at which the bubble was inflated. For $z_0 \sim 10$ kpc, the bubble will rise to 50 kpc.

Let us consider an AGN that inflates a sequence of bubbles. We can write the time-averaged mass outflow rate from the cluster centre due to a train of bubbles as

$$\dot{M}_{\mathrm{out}} \approx qM_{\mathrm{dis},0}/\tau, \tag{50}$$

where $\tau$ is the average time between bubble inflation. Since this outflow counteracts the inflow due to cooling, cumulatively bubble mass transport may allow for the relaxing of the stringent (but commonly adopted) requirement that AGN heating must balance radiative cooling. In fact, there is some debate as to whether AGN heating in fact balances cooling, especially in the most luminous clusters. Estimates of the time-averaged heating rate by Best et al. (2007), for example, indicates that AGN heating *does not* balance cooling in the most luminous clusters.[3] As we show below, mass outflow can play an important role in limiting the mass build-up at the cluster centre in such instances.

To illustrate this, let us consider the following: in the absence of heating, the mass inflow rate due to cooling is related to the radiative losses of the ICM according to

$$\dot{M}_{\mathrm{cool},0} = \frac{(\Gamma_{\mathrm{ICM}} - 1)}{\Gamma_{\mathrm{ICM}}} \frac{\mu m_{\mathrm{p}}}{k_{\mathrm{B}} T} L_{\mathrm{X}}, \tag{51}$$

where $T$ is the average temperature of the ICM. Studies of the X-ray spectra of the ICM in cluster cores indicate that the actual rate at which the gas is cooling is $\dot{M}_{\mathrm{cool}} \lesssim 0.2 \dot{M}_{\mathrm{cool},0}$ (e.g. Peterson et al. 2001; Kaastra et al. 2001; Peterson et al. 2003). If the mass inflow rate is balanced by the mass transport rate by the bubbles: $\dot{M}_{\mathrm{cool}} \approx \dot{M}_{\mathrm{out}}$.

The actual gas cooling rate, $\dot{M}_{\mathrm{cool}}$, is the result of a difference between cooling and heating:

$$\dot{M}_{\mathrm{cool}} = \frac{(\Gamma_{\mathrm{ICM}} - 1)}{\Gamma_{\mathrm{ICM}}} \frac{\mu m_{\mathrm{p}}}{k_{\mathrm{B}} T} \left( L_{\mathrm{X}} - \dot{E}_{\mathrm{heat}} \right), \tag{52}$$

where $\dot{E}_{\mathrm{heat}} = \alpha_{\mathrm{heat}} E_{\mathrm{bub},0}/\tau$. Here, $E_{\mathrm{bub},0}$ is the enthalpy of

[3] We note that Dunn & Fabian (2008) claim a close balance between heating and cooling but in their comparison, they refer to the heating rate due to an individual bubble. Averaging over the time between successive bubbles will lower the power estimate, leading to a discrepancy between heating and cooling in agreement with Best et al. (2007).

an AGN-inflated bubble (see equation 3) and $\alpha_{\rm heat}$ allows for the possibility that the bubble enthalpy may under-represent the total energy injected by the AGN (e.g. Nusser et al. 2006; Binney et al. 2007), especially if the bubbles are inflated supersonically, which would engender shocks that enhance the heating.

Combining equations (50)—(52) and taking $\Gamma_{\rm ICM} = 5/3$, $\Gamma_{\rm b} = 4/3$ and $T/T_0 \sim 3$, we find that the build-up of excessive amounts of cold gas in the central galaxy can be prevented if

$$\dot{E}_{\rm heat} \approx \frac{\alpha_{\rm heat}}{[2q + \alpha_{\rm heat}]} L_{\rm X} \tag{53}$$

and

$$\dot{M}_{\rm out} \approx \frac{2q}{[2q + \alpha_{\rm heat}]} \dot{M}_{\rm cool,0}. \tag{54}$$

If the AGN does no heating (i.e. $\alpha_{\rm heat} = 0$), mass transport by the wake can, by itself, prevent rate of cold gas in the central cluster galaxy as long as the bubble recurrence timescale is

$$\tau \approx 1 \times 10^7 \left(\frac{E_{\rm bub,0}}{10^{59}\,{\rm erg}}\right)\left(\frac{L_{\rm X}}{10^{44}\,{\rm erg\,s^{-1}}}\right)^{-1} {\rm yrs}, \tag{55}$$

where $10^{59}$ erg is the typical enthalpy of bubbles in a cluster with luminosity $L_{\rm X} \sim 10^{44}\,{\rm ergs^{-1}}$ (e.g. Bîrzan et al. 2004; Dunn et al. 2005) and we have taken $q \approx 0.24$. Of course, the corresponding $\dot{M}_{\rm cool}$ will exceed the limits derived from the X-ray spectra.

If, in addition to mass transport, the bubbles also heat the ICM such that the amount of energy deposited in the ICM is twice the enthalpy of the bubble (i.e. $\alpha_{\rm heat} = 2$), the rate of cold gas build-up can be prevented if the bubbles are inflated on a timescale

$$\tau \approx 5 \times 10^7 \left(\frac{E_{\rm bub,0}}{10^{59}\,{\rm erg}}\right)\left(\frac{L_{\rm X}}{10^{44}\,{\rm erg\,s^{-1}}}\right)^{-1} {\rm yrs}. \tag{56}$$

It is worth noting that in this particular case, the time-averaged heating rate does not balance the cooling rate, $\dot{E}_{\rm heat} \approx 0.8 L_{\rm X}$, and the mass cooling rate is the maximum allowed, $\dot{M}_{\rm cool} \approx 0.2 \dot{M}_{\rm cool,0}$, but mass build-up in the central cluster galaxy is successfully avoided by mass transport due to the bubbles.

The values of $\tau$ obtained from equation (56) are reasonably consistent with indirect observational estimates, though there are large uncertainties. For example, Best et al. (2007) found radio AGN duty cycles of $\sim 30\%$ in Brightest Cluster Galaxies (BCGs), which corresponds to an typical 'observed' time between outbursts of $\tau_{\rm obs} \sim 3 t_{\rm on}$, where $t_{\rm on}$ is the duration of an AGN outburst. Therefore, since $t_{\rm on}$ seems to vary between $10^7 - 10^8$ yrs (e.g. Bîrzan et al. 2004), it seems possible that AGN-blown bubbles can significantly reduce the rate at which cold gas collects in the galaxy.

Finally, we note that throughout this work we have only considered bubbles that remain intact. Bubbles which deform into vortex rings behave somewhat differently. In addition, the fluid circulation associated with the vortex ring exerts a force that can lift up additional material behind the bubble, (see Pavlovski et al. 2007). However, with the possible exception of M87 (Owen et al. 2000) structures resembling vortex rings have not been observed, so this additional mechanism of mass transport might be unimportant except in rare cases.

## 7 SUMMARY

The aim of this article is to provide a better understanding of the mass transport processes that are attributable to AGN-blown bubbles in clusters of galaxies. Recently observed filaments of cool material behind AGN-blown bubbles (e.g. Conselice et al. 2001; Crawford et al. 2005; Hatch et al. 2006) provide a strong indication that bubble-induced mass transport is operating at least within 10s of kiloparsecs of the cluster centre. The filaments likely represent only a fraction of the actual mass transported by the bubbles and some of this mass can be carried out to $\sim 50 - 100$ kiloparsecs.

Mass transport by AGN-inflated bubbles not only impacts bubble dynamics — including the rate at which the bubble expands as it rises — and the efficiency with which the bubble will heat its surroundings, it also removes the amount of cool gas available for star formation in the central galaxy, alleviating the stringent requirement that AGN heating balance radiative cooling. The system can tolerate a lower heating rate, implying that the systems identified by Best et al. (2007), in which the average heating rates fall short of the cooling rates, may still be balanced. For all these reasons, a better understanding of mass transport by the bubbles is important. In this paper, we have focused on three main mass transport mechanisms: drift, wake transport and entrainment.

- **Drift:** drift arises when an ascending bubble imparts an impulse on the ambient ICM ahead of it, causing a net upward displacement of the ambient material behind the bubble. In a gravitationally stratified environment, the material in the drift does not keep up with the bubble. It slows down and may even fall back to its original position.
- **Wake transport:** a rising, deformable bubble also forms a cavity (wake) at the rear of the bubble. The wake is filled with some of the ambient medium displaced when the bubble first starts to rise, and this material will be transported outward as the bubble rises.
- **Entrainment:** during formation and possibly, during the rise phase, some of the ambient ICM may be incorporated into the bubble body. This process is referred to as entrainment. The displacement of the bubble to larger radii in the cluster results in the transport of this entrained material.

Our most important findings regarding the above three processes can be summarized as follows:

(i) The upward displacement of the cool gas at the cluster centre in the form of drift offers a compelling explanation for the recently discovered cool filaments observed to be stretching between AGN-inflated bubbles and the cluster centre. The kinematic character of the filaments agrees well with the expected kinematic signature of drift. Our estimate of a drift mass of $\sim 10^8\,{\rm M}_\odot$ also agrees well with the estimate of mass in the cool filaments. We generically expect such filaments to form in clusters that either have entropy profiles that increase with radius (as is common in classical

cooling core clusters) or had such an entropy profile at the time when the bubble started its ascent.

(ii) The wake is the most promising mechanism for transporting material out of the cluster centre and out to distances of $\sim$ 100 kpc, depending on where the bubble is inflated and the ICM's radial density profile. (In the absence of the wake, the equilibrium radius of the very same bubble greatly exceeds the cluster's virial radius.) Our estimates suggest that typically a bubble will lift $\sim 10^8\,\mathrm{M}_\odot$ in its wake, which significantly weighs down the bubble. A hot air balloon with a weighted basket is an apt metaphor. This additional mass not only limits the maximum radius to which a bubble can rise but also significantly reduces the energy that can be extracted from the bubble. In a classical cool core cluster, a weighted bubble will deposit into the ICM only $\sim 18\%$ of the energy released associated with an unweighted bubble.

(iii) Brüggen et al. (2009) recently suggested that entrainment and projection effects may provide an explanation for the large apparent opening angles subtended by AGN-inflated bubbles. The presence of entrained material *does* increase the bubble's expansion rate. However, the entrainment rate required to account for the observations would also rapidly reduce the density contrast between the bubble and its surroundings. In a typical cluster, a bubble would only need to rise a distance equivalent to the initial bubble radius before it would become indistinguishable from its surroundings. Since Bîrzan et al. (2004) find numerous bubbles located more than 20 kpc from the cluster centres, we conclude that the bubble does not entrain material efficiently. There are two related implications: firstly, the large opening angle must be due to some other process, such as current-dominated AGN outflow model (e.g. Nakamura et al. 2006) as well as possible projection effects, as suggested by Brüggen et al. (2009). Secondly, some phenomenon prevents the formation of normal hydrodynamic instabilities and, therefore, suppresses entrainment. As a possible resolution, we note that bubble whose surface is draped by magnetic fields would behave as required. Whether such a bubble would be consistent with other constraints is a subject for further explorations.

(iv) With the introduction of mass transport of gas out of the cluster centre by the bubble, we find the clusters of galaxies can tolerate an average heating rate that is less than the cooling rate, which according to Best et al. (2007) is a common occurrence in luminous clusters, and prevent gas build-up in the central galaxy. The outward mass transport rate is largely determined by the wake mass and by the average time between bubble inflation. Typically, the bubble recurrence timescale is $\tau \sim 10^7$—$10^8$ yrs, which is reasonably consistent with observational estimates.

## 8 ACKNOWLEDGEMENTS

ECDP would like to thank the Department of Foreign Affairs and International Trade for funding through a Government of Canada Post-Doctoral Research Fellowship and CITA for funding through a National Fellowship. He would also like to acknowledge informative discussions with Jim Hinton and Ian Eames. GP thanks the STFC for financial support. AB acknowledges research support from NSERC through the Discovery Program and also expresses his gratitude to J. Criswick for his generous support. AD thanks CITA for financial support through a National Fellowship and an NSERC grant to Don VandenBerg is also acknowledged. The authors wish to thank the anonymous referee for insightful comments that improved this work.

## APPENDIX A: LIST OF PARAMETERS AND THEIR DEFINITIONS

| Parameter | Definition |
|---|---|
| $E_{\rm bub,0}$ | bubble enthalpy immediately after inflation |
| $P$ | pressure (bubble and ICM are in pressure equilibrium) |
| $P_0$ | pressure where bubble was inflated |
| $V_{\rm bub}$ | bubble volume |
| $V_{\rm bub,0}$ | initial bubble volume |
| $\rho_{\rm bub}$ | bubble density |
| $\rho_{\rm bub,0}$ | initial bubble density |
| $T_{\rm bub}$ | bubble temperature |
| $\Gamma_{\rm b}$ | bubble adiabatic index |
| $\Gamma_{\rm b,0}$ | initial bubble adiabatic index |
| $\rho_{\rm ICM}$ | ICM density |
| $\rho_{\rm ICM,0}$ | central ICM density |
| $\rho_0$ | ICM density where the bubble was inflated |
| $T_{\rm ICM}$ | ICM temperature |
| $T_0$ | ICM temperature where bubble was inflated |
| $T_1, T_2, z_{\rm T}$ | parameters for fit to ICM temperature profile |
| $\Gamma_{\rm ICM}$ | ICM adiabatic index |
| $\eta_0$ | defined as $\rho_0/\rho_{\rm bub,0}$ |
| $\eta_{\rm eff}$ | effective density contrast for bubble and wake system |
| $\eta_{\rm eff,0}$ | effective density contrast for bubble and wake system at the beginning of the rise phase |
| $\beta$ | exponent for $\beta$-law ICM density |
| $z$ | radial coordinate of cluster |
| $z_{\rm ICM,0}$ | scale height of $\beta$-law ICM density |
| $z_0$ | height at which the bubble is inflated |
| $z_{\rm eq}$ | height at which effective density of the bubble/wake systems equals the ICM density |
| $P(z_{\rm eq})$ | pressure at $z_{\rm eq}$ |
| $T_{\rm ICM}(z_{\rm eq})$ | ICM temperature at $z_{\rm eq}$ |
| $V_{\rm drift}$ | drift volume |
| $V_{\rm wake}$ | wake volume |
| $M_{\rm bub}$ | bubble mass |
| $M_{\rm dis}$ | ICM mass displaced by bubble |
| $M_{\rm dis,0}$ | initial ICM mass displaced by bubble |
| $M_{\rm wake}$ | mass of bubble wake |
| $q$ | fraction of initial displaced mass in the wake |
| $k$ | ratio of drift and bubble volumes |
| $g$ | gravitational acceleration |
| $w$ | bubble velocity |
| $w_{\rm terminal}$ | terminal bubble velocity |
| $r$ | bubble radius |
| $r_0$ | initial bubble radius |
| $a_{\rm bub}$ | bubble surface area |
| $\epsilon$ | turbulent energy dissipation rate per unit mass |
| $N$ | Brunt-Väisälä frequency |

| Parameter (cont...) | Definition |
|---|---|
| $\sigma$ | entropy index of ICM |
| $C_{\rm D}$ | drag coefficient for bubble |
| $L_{\rm O}$ | Ozmidov length |
| $L_{\rm buoy}$ | buoyancy length |
| $L$ | entrainment length |
| $c_{\rm turb}$ | numerical turbulence constant |
| $c_{\rm term}$ | drag coefficient-dependent |
| $Re$ | Reynolds number |
| $n$ | number of computational cells |
| $\alpha$ | entrainment coefficient |
| $\Gamma_{\rm i}$ | current bubble adiabatic index |
| $f_{\rm i}$ | fraction of bubble pressure contributed by entrained material |
| $\Delta V$ | volume increment of entrained material |
| $\Delta M$ | mass increment of entrained material |
| $\Delta V_{\rm i}$ | volume entrained during $i$th timestep |
| $V_{\rm i}$ | bubble volume in $i$th timestep |
| $\Gamma$ | effective adiabatic index |
| $c_{\rm p,bub}$ | specific heat at constant pressure of bubble |
| $c_{\rm p,ICM}$ | specific heat at constant pressure of ICM |
| $\theta$ | opening angle of bubble |
| $L_{\rm X}$ | X-ray luminosity of ICM |
| $T$ | characteristic temperature of ICM |
| $\dot{M}_{\rm cool,0}$ | classical mass flow rate associated with $L_{\rm X}$ and $T$ |
| $\dot{M}_{\rm cool}$ | the actual cooling flow |
| $\alpha_{\rm heat}$ | multiple of bubble enthalpy that represents total energy injected by AGN |
| $\tau$ | average time between bubbles being inflated |
| $\tau_{\rm obs}$ | observationally-determined time between bubbles being inflated |
| $t_{\rm on}$ | duration of an AGN outburst |
| $k_{\rm B}$ | Boltzman constant |
| $\mu m_{\rm p}$ | mean mass per particle |
| $A$ | cross-sectional area of bubble |

## REFERENCES


Allen S. W., Schmidt R. W., Fabian A. C., 2001, MNRAS, 328, L37

Bîrzan L., Rafferty D. A., McNamara B. R., Wise M. W., Nulsen P. E. J., 2004, ApJ, 607, 800

Babul A., Balogh M. L., Lewis G. F., Poole G. B., 2002, MNRAS, 330, 329

Benson A. J., Babul A., 2009, MNRAS, 397, 1302

Benson A. J., Bower R. G., Frenk C. S., Lacey C. G., Baugh C. M., Cole S., 2003, ApJ, 599, 38

Best P. N., von der Linden A., Kauffmann G., Heckman T. M., Kaiser C. R., 2007, MNRAS, 379, 894

Binney J., Bibi F. A., Omma H., 2007, MNRAS, 377, 142

Bower R. G., Benson A. J., Malbon R., Helly J. C., Frenk C. S., Baugh C. M., Cole S., Lacey C. G., 2006, MNRAS, 370, 645

Bower R. G., McCarthy I. G., Benson A. J., 2008, MNRAS, 390, 1399

Brüggen M., Scannapieco E., Heinz S., 2009, MNRAS, pp 479–+

Cavagnolo K. W., Donahue M., Voit G. M., Sun M., 2009, ApJ Supp., 182, 12

Choudhuri A., 1998, The Physics of Fluids and Plasmas, an introduction for astrophyisicists. Cambridge University Press

Churazov E., Böhringer H., Brüggen M., Forman W., Jones C., Kaiser C., Sunyaev R., 2002, in Gilfanov M., Sunyeav R., Churazov E., eds, Lighthouses of the Universe: The Most Luminous Celestial Objects and Their Use for Cosmology Bubble-Heated Cooling Flows. pp 37–+

Churazov E., Brüggen M., Kaiser C. R., Böhringer H., Forman W., 2001, ApJ, 554, 261

Churazov E., Sazonov S., Sunyaev R., Forman W., Jones C., Böhringer H., 2005, MNRAS, 363, L91

Churazov E., Sunyaev R., Forman W., Böhringer H., 2002, MNRAS, 332, 729

Conselice C. J., Gallagher III J. S., Wyse R. F. G., 2001, ApJ, 122, 2281

Crawford C. S., Sanders J. S., Fabian A. C., 2005, MNRAS, 361, 17

Croton D. J., Springel V., White S. D. M., De Lucia G., Frenk C. S., Gao L., Jenkins A., Kauffmann G., Navarro J. F., Yoshida N., 2006, MNRAS, 365, 11

Crowe C., 2005, Multiphase flow handbook. CRC Press

Crowe C., Sommerfeld S., Tsuji Y., 1998, Multiphase flows with droplets and particles. CRC Press

Dabiri J. O., 2006, Journal of Fluid Mechanics, 547, 105

Darwin C., 1953, Proc. Camb. Phil. Soc.

Davé R., Oppenheimer B. D., Sivanandam S., 2008, MNRAS, 391, 110

David L. P., Nulsen P. E. J., McNamara B. R., Forman W., Jones C., Ponman T., Robertson B., Wise M., 2001, ApJ, 557, 546

De Young D., 2006, Astron. Nach., 327, 231

De Young D. S., 2003, MNRAS, 343, 719

Dennis T. J., Chandran B. D. G., 2005, ApJ, 622, 205

Diehl S., Li H., Fryer C. L., Rafferty D., 2008, ApJ, 687, 173

Donahue M., Horner D. J., Cavagnolo K. W., Voit G. M., 2006, ApJ, 643, 730

Dunn R. J. H., Fabian A. C., 2008, MNRAS, 385, 757

Dunn R. J. H., Fabian A. C., Taylor G. B., 2005, MNRAS, 364, 1343

Dursi L. J., Pfrommer C., 2008, ApJ, 677, 993

Eames I., Gilbertson M A., 2005, Powder technology, 154, 185

Eames I., Gobby D., Dalziel S. B., 2003, Journal of Fluid Mechanics, 485, 67

Enßlin T. A., Heinz S., 2002, A&A, 384, L27

Gardini A., 2007, A&A, 464, 143

Ghizzardi S., Molendi S., Pizzolato F., De Grandi S., 2004, ApJ, 609, 638

Hatch N. A., Crawford C. S., Johnstone R. M., Fabian A. C., 2006, MNRAS, 367, 433

Hinton J. A., Domainko W., Pope E. C. D., 2007, MNRAS, 382, 466
Kaastra J. S., Ferrigno C., Tamura T., Paerels F. B. S., Peterson J. R., Mittaz J. P. D., 2001, A&A, 365, L99
Kaiser C. R., Pavlovski G., Pope E. C. D., Fangohr H., 2005, MNRAS, 359, 493
Kantha L. H., Clayson C. A., 2000, Small Scale Processes in Geophysical Fluid Flows, Volume 67. Academic Press
Landau L., Lifschitz E., 1995, Fluid Mechanics. Butterworth-Heinemann Ltd
Mathews W. G., Brighenti F., Buote D. A., Lewis A. D., 2003, ApJ, 596, 159
McCarthy I. G., Babul A., Bower R. G., Balogh M. L., 2008, MNRAS, 386, 1309
McCarthy I. G., Balogh M. L., Babul A., Poole G. B., Horner D. J., 2004, ApJ, 613, 811
McNamara B. R., 2002, in Schlegel E. M., Vrtilek S. D., eds, The High Energy Universe at Sharp Focus: Chandra Science Vol. 262 of Astronomical Society of the Pacific Conference Series, Clusters of Galaxies at Sharp Focus: Cooling Flows and Radio Sources Unveiled by Chandra. pp 351–+
McNamara B. R., Nulsen P. E. J., 2007, ARA&A, 45, 117
Milne-Thompson L., 1996, Theoretical hydrodynamics. Dover publications
Nakamura M., Li H., Li S., 2006, ApJ, 652, 1059
Nulsen P. E. J., Jones C., Forman W. R., David L. P., McNamara B. R., Rafferty D. A., Bîrzan L., Wise M. W., 2007, in Böhringer H., Pratt G. W., Finoguenov A., Schuecker P., eds, Heating versus Cooling in Galaxies and Clusters of Galaxies AGN Heating Through Cavities and Shocks. pp 210–+
Nusser A., Silk J., Babul A., 2006, MNRAS, 373, 739
Omma H., Binney J., Bryan G., Slyz A., 2004, MNRAS, 348, 1105
Owen F. N., Eilek J. A., Kassim N. E., 2000, ApJ, 543, 611
Pavlovski G., Kaiser C. R., Pope E. C. D., 2007, ArXiv e-prints
Pavlovski G., Kaiser C. R., Pope E. C. D., Fangohr H., 2008, MNRAS, 384, 1377
Peterson J. R., Kahn S. M., Paerels F. B. S., Kaastra J. S., Tamura T., Bleeker J. A. M., Ferrigno C., Jernigan J. G., 2003, ApJ, 590, 207
Peterson J. R., Paerels F. B. S., Kaastra J. S., Arnaud M., Reiprich T. H., Fabian A. C., Mushotzky R. F., Jernigan J. G., Sakelliou I., 2001, A&A, 365, L104
Pope E. C. D., 2009, MNRAS, pp 494–+
Pope E. C. D., 2010, ArXiv e-prints
Pope E. C. D., Hartquist T. W., Pittard J. M., 2008, MNRAS, 389, 1259
Pope E. C. D., Pavlovski G., Kaiser C. R., Fangohr H., 2006, MNRAS, 367, 1121
Puchwein E., Sijacki D., Springel V., 2008, ApJ, 687, L53
Rafferty D. A., McNamara B. R., Nulsen P. E. J., Wise M. W., 2006, ApJ, 652, 216
Revaz Y., Combes F., Salomé P., 2008, A&A, 477, L33
Reynolds C. S., McKernan B., Fabian A. C., Stone J. M., C. V. J., 2004, MNRAS: submitted., p. 11
Robinson K., Dursi L. J., Ricker P. M., Rosner R., Calder A. C., Zingale M., Truran J. W., Linde T., Caceres A., Fryxell B., Olson K., Riley K., Siegel A., Vladimirova N., 2004, ApJ, 601, 621
Roediger E., Brüggen M., Rebusco P., Böhringer H., Churazov E., 2007, MNRAS, 375, 15
Salomé P., Combes F., Edge A. C., Crawford C., Erlund M., Fabian A. C., Hatch N. A., Johnstone R. M., Sanders J. S., Wilman R. J., 2006, A&A, 454, 437
Salomé P., Revaz Y., Combes F., Pety J., Downes D., Edge A. C., Fabian A. C., 2008, A&A, 483, 793
Sanders J. S., Fabian A. C., 2007, in Böhringer H., Pratt G. W., Finoguenov A., Schuecker P., eds, Heating versus Cooling in Galaxies and Clusters of Galaxies Hard X-ray emission from the core of the Perseus cluster and the thermal content of the radio bubbles. pp 74–+
Sanderson A. J. R., O'Sullivan E., Ponman T. J., 2009, MNRAS, 395, 764
Schetz J., Fuhs A., 1999, Fundamentals of fluid mechanics. Wiley-Interscience
Shen C., 2005, Rarefied Gas Dynamics: Fundamentals, Simulations and Micro Flows (Heat and Mass Transfer). Springer
Silk J., Rees M. J., 1998, A&A, 331, L1
Turner J. S., 1969, Annual Review of Fluid Mechanics, 1, 29
Turner J. S., 1986, Journal of Fluid Mechanics, 173, 431
Yang W., 2003, Handbook of fluidization and fluid-particle systems. CRC Press